

Online Identification of IT Systems through Active Causal Learning

Kim Hammar and Rolf Stadler

KTH Royal Institute of Technology, Sweden

Email: kimham@kth.se and stadler@kth.se

September 3, 2025

Abstract—Identifying a causal model of an IT system is fundamental to many branches of systems engineering and operation. Such a model can be used to predict the effects of control actions, optimize operations, diagnose failures, detect intrusions, etc., which is central to achieving the longstanding goal of automating network and system management tasks. Traditionally, causal models have been designed and maintained by domain experts. This, however, proves increasingly challenging with the growing complexity and dynamism of modern IT systems. In this paper, we present the first principled method for online, data-driven identification of an IT system in the form of a causal model. The method, which we call *active causal learning*, estimates causal functions that capture the dependencies among system variables in an iterative fashion using Gaussian process regression based on system measurements, which are collected through a rollout-based intervention policy. We prove that this method is optimal in the Bayesian sense and that it produces effective interventions. Experimental validation on a testbed shows that our method enables accurate identification of a causal system model while inducing low interference with system operations.

I. INTRODUCTION

SIGNIFICANT progress in autonomous management of IT systems is required to achieve reliable operation and predictable service quality as these systems are becoming increasingly complex and dynamic. Efforts towards automating the management of networks and IT systems have been undertaken over the last 30 years, initially motivated by the lack of experts who could reliably configure and maintain these increasingly capable systems and technologies. Starting with policy-based management in the 1990s (e.g., [1]), a series of paradigms have been proposed and developed, often initiated by industry and then studied in collaboration with academia. These efforts include autonomic management (e.g., [2]), self-organizing networks (e.g., [3]), intent-based network management (e.g., [4]), and zero-touch management (e.g., [5]). A comprehensive overview of these developments from a networking perspective is provided by Coronado et al. [6].

We advocate for a principled approach to autonomous management that is based on a formal foundation. Specifically, we propose to construct and maintain a *causal model* of an IT system under consideration. The formal concept of causality and the theory of causal models that we use in this paper have been established in the seminal work by Pearl and collaborators [7], [8], and the connection to machine learning has been investigated more recently by Peters et al. [9].

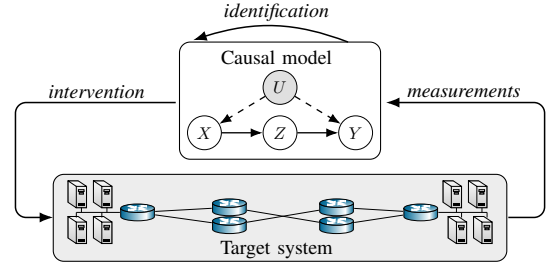


Fig. 1: Online identification of IT systems through active causal learning.

A causal model of an IT system captures the causal relations between key variables that characterize the system’s infrastructure (e.g., the available memory), its services (e.g., the response time of a service request), and external factors (e.g., the load generated by users of the services). Knowing the causal model of an IT system allows to predict how the system will react to a control action, such as scaling the CPU allocation, or to a change in an external factor, such as the service load. It allows building autonomous resource allocation functions that achieve management objectives in a changing environment. Also, it provides a formal understanding of the system dynamics and their relation to management objectives.

Such a model is defined by a directed graph, called the *causal graph*, which expresses the causal dependencies among system variables, and by a set of *causal functions*, which capture the functional dependencies among the variables. Since causal dependencies can often be deduced from the hardware and software architecture of the system and since they seldom change during operation, we assume in this paper that the causal graph is known, and we focus on identifying the causal functions of a causal model that represents the IT system. Specifically, we present an *online* method for identifying the causal functions of an IT system and for updating them over time. We call this method *active causal learning*.

In our method, we learn the causal model in an iterative manner by combining continuous monitoring with a sequence of interventions on the IT system; see Fig. 1. During an intervention, we set one or more control variables of the system to new values and measure the resulting change in the system variables. For example, an intervention in this context may be to temporarily adjust the CPU limit of a service and observe how this change affects response times of service requests. By combining interventions with continuous

monitoring, we can obtain measurement samples across the system’s (complete) *operating region*, i.e., the combinations of workloads and configurations of control variables under which the system is designed to operate [10]; see Fig. 2.

Using the measurements up to the current time, we produce a new estimate of the causal model after each monitoring interval. Specifically, we estimate the causal functions of the IT system through Gaussian process (GP) regression. This approach allows us to quantify the uncertainty in the current estimates, which we use to guide the selection of interventions. We show that the problem of selecting interventions that reduce model uncertainty while having a low operational cost can be formulated as a dynamic programming problem. Solving this problem is computationally challenging as the number of possible interventions grows exponentially with the number of system variables. Moreover, evaluating the expected effect of an intervention involves computing high-dimensional integrals. We address these challenges by designing an efficient rollout algorithm for approximating optimal intervention policies through lookahead optimization.

We prove that our method is optimal in the Bayesian sense and establish conditions under which our rollout algorithm produces effective interventions. We evaluate the method in a testbed where we set up an IT system with two web services based on a microservice architecture. During operation of this system, we continually estimate its causal model and use it to predict service response times in function of control variable settings. The experimental results are consistent with our theoretical claims and show that our method can closely track the evolving model of a dynamic system.

The main contributions of this paper are:

- We present the first principled method for online, data-driven identification of an IT system, which we call *active causal learning*. The method estimates a causal model of the system in an iterative fashion, involving GP regression, rollout, and lookahead optimization.
- We prove that our method is optimal in the Bayesian sense and produces effective intervention policies.
- We experimentally validate the method on a testbed [11]. The results show that it enables efficient and accurate identification of a causal system model while inducing low interference with system operations.

II. EXAMPLE USE CASE: PERFORMANCE OBJECTIVES

Consider an IT system that provides network services to a client population. Continuously meeting performance objectives for these services requires the system to periodically take control actions, such as scaling resources when the load increases, or relocating network functions in response to failures of system components. To automate the selection of such actions, a model is required that captures how changes to certain system variables (e.g., CPU allocations) affect changes in others (e.g., response times). In other words, the model must convey cause-and-effect relationships among system variables.

Such causal relationships are governed by complex interactions among system components and further depend on external factors. For example, relocating a network function

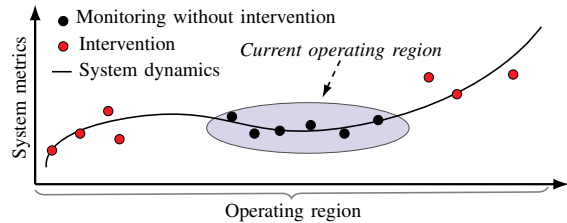


Fig. 2: Comparison between data collection with and without interventions. Monitoring the system without interventions yields measurements only within the system’s *current* operating region [12], while interventions allow for collecting measurement samples across the (complete) operating region.

to mitigate a failure may improve service availability while, at the same time, increasing latency or congestion in other parts of the network. Moreover, these causal relationships are time-varying and dependent on underlying hardware architectures.

III. PROBLEM STATEMENT

We consider the problem of identifying a causal model of an IT system based on measurement data from the system. We assume that causal dependencies among the system variables are known and expressed in the form of a *causal graph* [7, Def. 2.2.1]. This graph encodes structural properties, which define a set of candidate models. Our goal is to identify the most suitable model within this set based on the available data. This data can be obtained either through monitoring or through interventions on specific system variables.

Since the system and its operating conditions may change over time, the identification must be performed *online* and involves two interconnected tasks: (i) estimating a causal model based on the available data; and (ii) selecting interventions for collecting new measurements. These tasks are carried out in an iterative process, where each new measurement informs the next model update. When designing this process, our goal is to track the evolution of the system while keeping intervention costs low. The next section formalizes this problem.

IV. THE ONLINE CAUSAL IDENTIFICATION PROBLEM

To define a causal model for an IT system, we adopt the formalism of structural causal models (SCM) [7, Def 7.1.1]. Following this formalism, we define the system model as

$$\mathcal{M}_t \triangleq \langle \mathbf{U}, \mathbf{V}, \mathbf{F}_t, \mathbb{P}[\mathbf{U}] \rangle, \quad t = 1, 2, \dots, \quad (1)$$

where \mathbf{U} and \mathbf{V} are finite sets of (real-valued) *exogenous* and *endogenous* random variables, respectively. The exogenous variables represent external factors such as the service load, while the endogenous ones describe internal system properties like response time. Among these variables, we distinguish between those that can be directly controlled (e.g., CPU allocation), denoted by \mathbf{X} , and those that cannot (e.g., the end-to-end response time of a service request), denoted by \mathbf{N} .

We assume that the sets \mathbf{U} and \mathbf{V} are chosen so that all possible configurations of the variables in $\mathbf{U} \cup \mathbf{V}$ define the system’s *operating region* [12], i.e., the set of configurations for which the system is intended to function. Formally,

Definition 1 (Operating region). *Given a structural causal model \mathcal{M}_t [cf. (1)] of an IT system, the system's (complete) operating region is given by*

$$\mathcal{O} \triangleq \mathcal{R}(\mathbf{U}) \times \mathcal{R}(\mathbf{V}),$$

where $\mathcal{R}(\cdot)$ denotes the range of a set of random variables.

Dependencies among variables are encoded in a (directed and acyclic) *causal graph* \mathcal{G} , whose nodes correspond to elements of $\mathbf{U} \cup \mathbf{V}$ and edges represent causal functions; see Fig. 3. Specifically, each endogenous variable V_i is determined by a *causal function* $f_{V_i,t}$, which maps its parent variables in the graph to its output value. For example, a causal function may take the form $R = f_{R,t}(L)$, where R represents response time and L represents system load. The collection of all such functions at time t is denoted by $\mathbf{F}_t \triangleq \{f_{V_i,t}\}_{V_i \in \mathbf{V}}$. We consider that these functions may evolve over time and that they are unknown. Further, we assume that the causal graph \mathcal{G} and the probability distribution $\mathbb{P}[\mathbf{U}]$ are fixed and known.

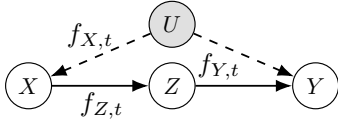


Fig. 3: A causal graph [7, Def. 2.2.1]; circles represent variables in an SCM; cf. (1); solid arrows represent causal dependencies between endogenous variables; dashed arrows represent causal dependencies on exogenous variables.

In the context of IT systems, samples of the variables $\mathbf{V} \cup \mathbf{U}$ correspond to logs and metrics measured on the target system. Following the formalism of SCMs, such samples can be drawn from any probability distribution from the set

$$\{\mathbb{P}[\mathbf{V}, \mathbf{U} \mid \text{do}(\mathbf{X}' = \mathbf{x}')] \mid \mathbf{X}' \in 2^{\mathbf{X}}, \mathbf{x}' \in \mathcal{R}(\mathbf{X}')\}, \quad (2)$$

where $2^{\mathbf{X}}$ is the powerset of \mathbf{X} , $\mathcal{R}(\mathbf{X}')$ is the range of \mathbf{X}' (i.e., the set of values \mathbf{X}' can take on), and $\text{do}(\mathbf{X}' = \mathbf{x}')$ represents an *atomic intervention* that temporarily fixes a set of variable(s) \mathbf{X}' to constant value(s) \mathbf{x}' irrespective of the functions \mathbf{F}_t [7, Def. 3.2.1]. We use the do operator as a mathematical representation of an intervention on the system.

In such an intervention, the system is configured according to $\mathbf{X}' = \mathbf{x}'$ and measurement samples are collected while the system operates under these imposed conditions. We assume that the samples are collected after the system has reached a steady state under these conditions, i.e., after the transient effects of the intervention have settled. For example, suppose the intervention modifies the routing configuration. In this case, the system is in a steady state when the changes in the routing tables have propagated through the network. Once sufficient data has been gathered in the steady state, the intervention is terminated and the system variables in the set \mathbf{X}' are restored to their pre-intervention values.

The special case $\text{do}(\emptyset)$ corresponds to the *passive intervention* without changing any control variables, i.e., observing the system in its *current operating region*, as defined next.

Definition 2 (Current operating region). *Given a structural causal model \mathcal{M}_t [cf. (1)] of an IT system, the current operat-*

ing region at time t is the set of feasible system configurations given the distribution $\mathbb{P}[\mathbf{U}]$ and the causal functions \mathbf{F}_t , i.e.,

$$\mathcal{O}_t \triangleq \left\{ (\mathbf{u}, \mathbf{v}) \in \mathcal{O} \mid \mathbb{P}[\mathbf{U} = \mathbf{u}] > 0, \mathbb{P}[\mathbf{V} = \mathbf{v} \mid \mathbf{u}, \mathbf{F}_t] > 0 \right\},$$

where \mathcal{O} is the (complete) operating region; cf. Def. 1.

The current operating region is generally a strict subset of the (complete) operating region, i.e., $\mathcal{O}_t \subset \mathcal{O}$. Consequently, relying solely on samples from \mathcal{O}_t is generally insufficient for constructing an accurate model across the complete operating region, which is the goal of system identification.

We model *online system identification* as a discrete-time process in which interventions and model updates occur at discrete points in time. Specifically, at each time $t = 1, 2, \dots$, one intervention can be performed, which yields M samples from one of the distributions in (2), where M is a configurable parameter. Let $\mathcal{D}_{\text{do}(\mathbf{X}' = \mathbf{x}'), t}$ denote the set of samples from the distribution $\mathbb{P}[\mathbf{V}, \mathbf{U} \mid \text{do}(\mathbf{X}' = \mathbf{x}')] from time 1 up to time t . The total dataset of samples up to time t is then the union$

$$\mathcal{D}_t \triangleq \bigcup_{\mathbf{X}' \in 2^{\mathbf{X}}, \mathbf{x}' \in \mathcal{R}(\mathbf{X}')} \mathcal{D}_{\text{do}(\mathbf{X}' = \mathbf{x}'), t}. \quad (3)$$

Given the evolving dataset \mathcal{D}_t , our goal is to sequentially estimate the causal functions \mathbf{F}_t ; cf. (1). That is, we aim to estimate a sequence of functions $\hat{\mathbf{F}}_1, \hat{\mathbf{F}}_2, \dots$ that are as close as possible to the true sequence $\mathbf{F}_1, \mathbf{F}_2, \dots$ while minimizing the cost of interventions. We formalize this objective as

$$\underset{(\text{do}(\mathbf{X}' = \mathbf{x}'), \hat{\mathbf{F}}_t)_{t \geq 1}}{\text{minimize}} \sum_{t=1}^{\infty} \gamma^{t-1} \left(\mathcal{L}(\hat{\mathbf{F}}_t, \mathbf{F}_t) + c(\text{do}(\mathbf{X}' = \mathbf{x}')) \right), \quad (4)$$

where $\gamma \in (0, 1)$ is a discount factor, $\text{do}(\mathbf{X}' = \mathbf{x}')$ is the intervention at time t , c is a cost function that encodes the cost of interventions, and \mathcal{L} is a loss function that quantifies the accuracy of the estimated causal functions. This bi-objective captures a trade-off between estimation accuracy and intervention cost, which can be controlled by tuning the cost function c and the loss function \mathcal{L} . In this paper, we consider the cost function c to be specific to the application use case, and we define the loss function \mathcal{L} as

$$\mathcal{L}(\hat{\mathbf{F}}_t, \mathbf{F}_t) \triangleq \sum_{V_i \in \mathbf{V}} \int_{\mathcal{R}(\text{pa}_{\mathcal{G}}(V_i))} \left(f_{V_i,t}(\mathbf{x}) - \hat{f}_{V_i,t}(\mathbf{x}) \right)^2 \mathbb{P}[\text{d}\mathbf{x}], \quad (5)$$

where $\text{pa}_{\mathcal{G}}(V_i)$ is the set of parents of the variable V_i in the graph \mathcal{G} , $f_{V_i,t} \in \hat{\mathbf{F}}_t$ is the estimated causal function of V_i , and $\mathbb{P}[\text{d}\mathbf{x}]$ represents the probability measure with respect to which the integral is calculated. For example, consider the variables X and U in Fig. 3. Suppose the distribution of the exogenous variable U admits a probability density function $p(u)$. Then the integral related to the endogenous variable X becomes

$$\int_{\mathcal{R}(U)} \left(f_{X,t}(u) - \hat{f}_{X,t}(u) \right)^2 p(u) \text{d}u.$$

The loss function \mathcal{L} [cf. (5)] quantifies the difference between the true causal functions $\mathbf{F}_t = \{f_{V_i,t}\}_{V_i \in \mathbf{V}}$ and the estimated causal functions $\hat{\mathbf{F}}_t = \{\hat{f}_{V_i,t}\}_{V_i \in \mathbf{V}}$, weighted by the probability distribution determined by the causal graph \mathcal{G} and

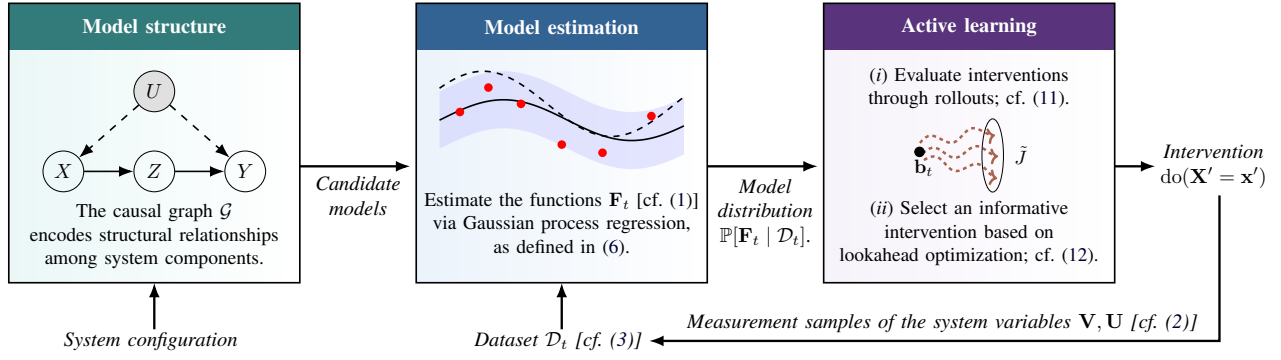


Fig. 4: Our iterative method for online identification of a causal model of an IT system. Such a model consists of a set of causal functions \mathbf{F}_t ; cf. (1). The set of candidate models is defined by a causal graph that encodes structural properties of the system. During an iteration, we fit a distribution over this set using system measurements and Gaussian processes. This distribution then guides the selection of the next intervention aimed at refining the distribution while keeping the intervention cost low. We implement this selection using rollout and lookahead optimization.

the distribution $\mathbb{P}[\mathbf{U}]$. (Recall that we assume that both the graph \mathcal{G} and the distribution $\mathbb{P}[\mathbf{U}]$ are known.)

Given these definitions and assumptions, we formally define the online causal identification problem as follows.

Problem (Online identification of an IT system)

Consider an IT system modeled by an SCM. The causal graph and the distribution $\mathbb{P}[\mathbf{U}]$ of this SCM are fixed and known, but the causal functions \mathbf{F}_t are unknown and may vary over time; cf. (1). The problem is to design an *estimator* $\varphi(\mathcal{D}_t)$ and an *intervention policy* $\pi(\mathcal{D}_t)$ for accurately tracking the causal functions \mathbf{F}_t , while keeping intervention costs low, as defined in (4).

V. OUR METHOD FOR ONLINE SYSTEM IDENTIFICATION

Our method for solving the problem in the preceding section consists of two parts: (i) Bayesian learning of the causal functions \mathbf{F}_t [cf. (1)] via Gaussian process regression; and (ii) selection of interventions for collecting measurement data via rollout and lookahead optimization; see Fig. 4.

A. Model Estimation through Gaussian Process Regression

In our method, we use Gaussian process (GP) regression to estimate the unknown causal functions of the target system [13, Def. 2.1]. Although the functions in \mathbf{F}_t are deterministic at each time t , we represent our uncertainty about them through a probability distribution over possible functions. Specifically, we place an independent GP prior on each of the causal functions $f_{V_i,t}$ in \mathbf{F}_t ; cf. (1). That is, before collecting any measurement data, we express our uncertainty about the causal function $f_{V_i,t}$ for every endogenous variable $V_i \in \mathbf{V}$ through the GP $\hat{f}_{V_i,t} \sim \mathcal{GP}(m_i, k_i)$, where $m_i(\mathbf{x}_i)$ is the mean function and $k_i(\mathbf{x}_i, \mathbf{x}'_i)$ is the covariance function. Here $\hat{f}_{V_i,t}(\mathbf{x}_i)$ is the estimated value of V_i given that its parents in the causal graph \mathcal{G} take on the values in the vector \mathbf{x}_i . Similarly, the variance $k_i(\mathbf{x}_i, \mathbf{x}'_i)$ represents the uncertainty about the estimated function $\hat{f}_{V_i,t}$ at the input vector \mathbf{x}_i . Finally, $k_i(\mathbf{x}_i, \mathbf{x}'_i)$ encodes the correlation between the function values at two different inputs: \mathbf{x}_i and \mathbf{x}'_i .

As the dataset \mathcal{D}_t [cf. (3)] is updated over time with new measurements, we update the GP prior of each causal function $\hat{f}_{V_i,t}$ via Bayes' rule; see Appendix D for detailed formulas of these updates. We denote the resulting posterior as $\hat{f}_{V_i,t} | \mathcal{D}_t \sim \mathcal{GP}(m_{i|\mathcal{D}_t}, k_{i|\mathcal{D}_t})$, where $m_{i|\mathcal{D}_t}$ and $k_{i|\mathcal{D}_t}$ denote the posterior mean and covariance functions given the dataset \mathcal{D}_t . This posterior allows us to predict $f_{V_i,t}(\mathbf{x}_i)$ using the mean $m_{i|\mathcal{D}_t}(\mathbf{x}_i)$, whose uncertainty is quantified by the variance $k_{i|\mathcal{D}_t}(\mathbf{x}_i, \mathbf{x}_i)$. Since we can make such predictions for any causal function $f_{V_i,t} \in \mathbf{F}_t$ and input $\mathbf{x}_i \in \mathcal{R}(\text{pa}_{\mathcal{G}}(V_i))$, the collection of all the posterior GPs $\{(\hat{f}_{V_i,t} | \mathcal{D}_t) | V_i \in \mathbf{V}\}$ allows to estimate the causal functions \mathbf{F}_t ; cf. (1). In particular, since the GPs are independent, we can construct a probability distribution over the causal functions \mathbf{F}_t according to

$$\varphi(\mathcal{D}_t) \triangleq \mathbb{P}[\mathbf{F}_t | \mathcal{D}_t] = \prod_{V_i \in \mathbf{V}} \mathbb{P}[f_{V_i,t} | \mathcal{D}_t], \quad (6)$$

where each distribution $\mathbb{P}[f_{V_i,t} | \mathcal{D}_t]$ is represented by a GP $\mathcal{GP}(m_{i|\mathcal{D}_t}, k_{i|\mathcal{D}_t})$. This distribution quantifies the uncertainty about the causal functions \mathbf{F}_t based on the dataset \mathcal{D}_t . To obtain a point estimate of the functions, we take the expectation with respect to this distribution, i.e., $\hat{\mathbf{F}}_t = \mathbb{E}_{\mathbf{F}_t \sim \varphi(\mathcal{D}_t)}\{\mathbf{F}_t\}$. This estimate of \mathbf{F}_t is optimal in the following sense.

Proposition 1. *The expectation $\mathbb{E}_{\mathbf{F}_t \sim \varphi(\mathcal{D}_t)}\{\mathbf{F}_t\}$ minimizes the expected value of the loss function \mathcal{L} [cf. (5)], i.e.,*

$$\mathbb{E}_{\mathbf{F}_t \sim \varphi(\mathcal{D}_t)}\{\mathbf{F}_t\} \in \arg \min_{\hat{\mathbf{F}}_t} \mathbb{E}_{\mathbf{F}_t \sim \varphi(\mathcal{D}_t)} \left\{ \mathcal{L}(\hat{\mathbf{F}}_t, \mathbf{F}_t) \right\},$$

where the minimization is over all sets of causal functions $\hat{\mathbf{F}}_t$ compatible with the causal graph \mathcal{G} .

We present the proof of Prop. 1 in Appendix B. This proposition expresses that the expectation $\mathbb{E}_{\mathbf{F}_t \sim \varphi(\mathcal{D}_t)}\{\mathbf{F}_t\}$ based on the estimator φ [cf. (6)] is Bayes-optimal. That is, among all SCMs that respect the structure encoded in the causal graph \mathcal{G} , this expectation yields the lowest expected value of the loss function \mathcal{L} ; cf. (5). In other words, it is the best prediction we can make for the causal functions \mathbf{F}_t given the data up to time t . In addition to the Bayes-optimality, the expectation $\mathbb{E}_{\mathbf{F}_t \sim \varphi(\mathcal{D}_t)}\{\mathbf{F}_t\}$ converges to the true causal functions given sufficient data and regularity, as stated below.

Proposition 2. Assume a) that the causal functions \mathbf{F} [cf. (1)] are fixed; and b) that the difference between each causal function $f_{V_i}(\mathbf{x}_i)$ and the (prior) mean function m_i lies in the reproducing kernel Hilbert space of the covariance function k_i . If each input $\mathbf{x}_i \in \mathcal{R}(\text{pa}_{\mathcal{G}}(V_i))$ is sampled infinitely often with independent zero-mean Gaussian noise, then

$$\lim_{|\mathcal{D}_i| \rightarrow \infty} \mathbb{E} \left\{ \left(\hat{f}_{V_i}(\mathbf{x}_i) - f_{V_i}(\mathbf{x}_i) \right)^2 \right\} = 0,$$

where $\hat{f}_{V_i} = \mathbb{E}_{\mathbf{F}_t \sim \varphi(\mathcal{D}_t)} \{f_{V_i}\}$ [cf. (6)] and the expectation is with respect to the sampling noise and variability.

Proposition 2 implies that the estimator φ [cf. (6)] recovers the true causal functions in the limit of infinite data, given certain regularity conditions. In other words, the estimator φ is *consistent*. This is a well-known result in GP theory, see e.g., [14, Thm. 3] for a detailed analysis and proof.

Remark 1. While the GP estimator φ [cf. (6)] is designed for continuous functions, it can also estimate functions over discrete domains by adapting the covariance function and restricting predictions to the discrete set; see [15] for details.

B. Active Learning through Rollout

Given the estimator φ of the causal functions \mathbf{F}_t [cf. (6)], the problem of active learning is to select a sequence of interventions that generate samples from the distributions (2) to update the dataset \mathcal{D}_t and achieve the objective (4). This problem can be formulated as a dynamic programming problem where the (belief) state is $\mathbf{b}_t \triangleq \varphi(\mathcal{D}_t)$, the control at time t is the intervention $u_t \triangleq \text{do}(\mathbf{X}'_t = \mathbf{x}'_t)$, the intervention policy is $\pi(\mathbf{b}_t)$, and the dynamics are defined as

$$\mathbf{b}_{t+1} \triangleq \varphi(\mathcal{D}_t \cup \{\mathbf{z}_t\}), \quad \text{for all } t \geq 1, \quad (7)$$

where \mathbf{z}_t is the measurement obtained after the intervention u_t ; cf. (2). The goal when selecting interventions is to improve the accuracy of the estimated functions $\hat{\mathbf{F}}_t$ while keeping the intervention costs $c(u)$ low; cf. (4). The accuracy of $\hat{\mathbf{F}}_t$ is quantified by the loss function \mathcal{L} , as defined in (5). However, \mathcal{L} cannot be directly computed as it depends on the unknown causal functions \mathbf{F} . For this reason, we define a *surrogate loss function* that captures the expected value of \mathcal{L} given the belief state \mathbf{b} . We denote this function by \mathcal{L} and define it as

$$\mathcal{L}(\mathbf{b}) \triangleq \int_{\mathcal{F}} \mathbf{b}(\mathbf{F}) \left(\mathcal{L}(\mathbf{F}, \mathbb{E}_{\mathbf{F}_t \sim \mathbf{b}} \{\mathbf{F}_t\}) \right) d\mathbf{F}, \quad (8)$$

where the integral is over the space of functions compatible with the causal graph \mathcal{G} . Minimizing this surrogate loss function reduces uncertainty in the belief state \mathbf{b} . In particular, $\mathcal{L}(\mathbf{b}) = 0$ if and only if $\mathbf{b}(\mathbf{F}) = 1$ for some set of causal functions \mathbf{F} . Moreover, by the consistency of the GP estimator φ [cf. Prop. 2], this condition implies that $\mathbf{F} = \mathbf{F}_t$. Hence, selecting interventions that drive the surrogate loss function $\mathcal{L}(\mathbf{b})$ to zero is equivalent to identifying the true causal functions and thus minimizing the loss function \mathcal{L} ; cf. (5).

Given the surrogate loss function \mathcal{L} , we define the cost function $g(\mathbf{b}, u)$ of the dynamic programming problem as

$$g(\mathbf{b}_t, u_t) \triangleq \mathbb{E}_{\mathbf{b}_{t+1}} \{ \mathcal{L}(\mathbf{b}_{t+1}) - \mathcal{L}(\mathbf{b}_t) \mid u_t, \mathbf{b}_t \} + c(u_t). \quad (9)$$

This cost function quantifies the expected change in the surrogate loss $\mathcal{L}(\mathbf{b})$ [cf. (8)] after performing the intervention u_t , collecting M measurement samples from the corresponding interventional distribution in (2), and updating the belief state \mathbf{b}_t using the GP estimator φ , as defined in (6). Hence, the structure of the cost function g aligns with the objective (4). Specifically, by selecting interventions that minimize the expected cost, we obtain an intervention policy that maximizes the expected reduction in uncertainty of the belief state \mathbf{b}_t [as quantified by the first term in (9)] while keeping the intervention cost low, as quantified by the second term in (9).

The solution to the dynamic program with the dynamics (7) and the cost function (9) yields an optimal intervention policy π^* , which minimizes the following cost-to-go function.

$$J_{\pi}(\mathbf{b}) \triangleq \lim_{T \rightarrow \infty} \mathbb{E}_{\pi} \left\{ \sum_{t=1}^T \gamma^{t-1} g(\mathbf{b}_t, u_t) \mid \mathbf{b}_1 = \mathbf{b} \right\}, \quad (10)$$

where \mathbb{E}_{π} denotes the expectation of $(\mathbf{b}_t)_{t \geq 2}$ when updating the dataset \mathcal{D}_t [cf. (3)] using the intervention policy π .

While (7) can be efficiently computed, (9) involves an integral [cf. (5)] that is intractable in general. Another challenge in solving this dynamic programming problem is that the dynamics (7) are non-stationary in case the underlying IT system evolves. In particular, the distribution of the measurement sample \mathbf{z}_t [cf. (2)] may become dependent on the time step t . For these reasons, the problem of computing an optimal intervention policy π^* is intractable in the general case.

To address this computational intractability, we approximate the cost function g [cf. (9)] by discretizing the function space \mathcal{F} [cf. (8)] and using Monte-Carlo sampling to estimate the expectation in (9). Moreover, we approximate an optimal intervention policy using *rollout*, which is an online methodology for approximate dynamic programming developed by Bertsekas; see textbook [16] and paper [17]. Following this methodology, at each time step t of the identification, we simulate the evolution of the dataset \mathcal{D}_t [cf. (3)] m time steps into the future, whereby interventions are selected according to a *base intervention policy* π . This lookahead simulation allows us to estimate the cost-to-go of the base policy as

$$\tilde{J}_{\pi}(\mathbf{b}_t) = \frac{1}{L} \sum_{j=1}^L \sum_{l=t}^{t+m-1} \gamma^{l-t} g(\mathbf{b}_l^j, \pi(\mathbf{b}_l^j)) + \gamma^m \tilde{J}(\mathbf{b}_{t+m}^j), \quad (11)$$

where L is the number of simulations and \tilde{J} is a function that approximates future costs. Both this function and the base policy π can be chosen freely, e.g., based on heuristics or offline optimization [18]–[20]. For example, they can be defined as $\pi(\mathbf{b}) = \text{do}(\emptyset)$ and $\tilde{J}(\mathbf{b}) = 0$ for all belief states \mathbf{b} .

Finally, we use the cost-to-go estimate obtained through (11) to transform the base policy to a *rollout policy* $\tilde{\pi}$ as

$$\tilde{\pi}(\mathbf{b}_t) \in \arg \min_{u_t} \left[g(\mathbf{b}_t, u_t) + \min_{\pi_{t+1}, \dots, \pi_{t+\ell-1}} \mathbb{E}_{\mathbf{b}_{t+1}, \dots, \mathbf{b}_{t+\ell}} \left\{ \sum_{j=t+1}^{t+\ell-1} \gamma^{j-t} g(\mathbf{b}_j, \pi_j(\mathbf{b}_j)) + \gamma^{\ell} \tilde{J}_{\pi}(\mathbf{b}_{t+\ell}) \right\} \right], \quad (12)$$

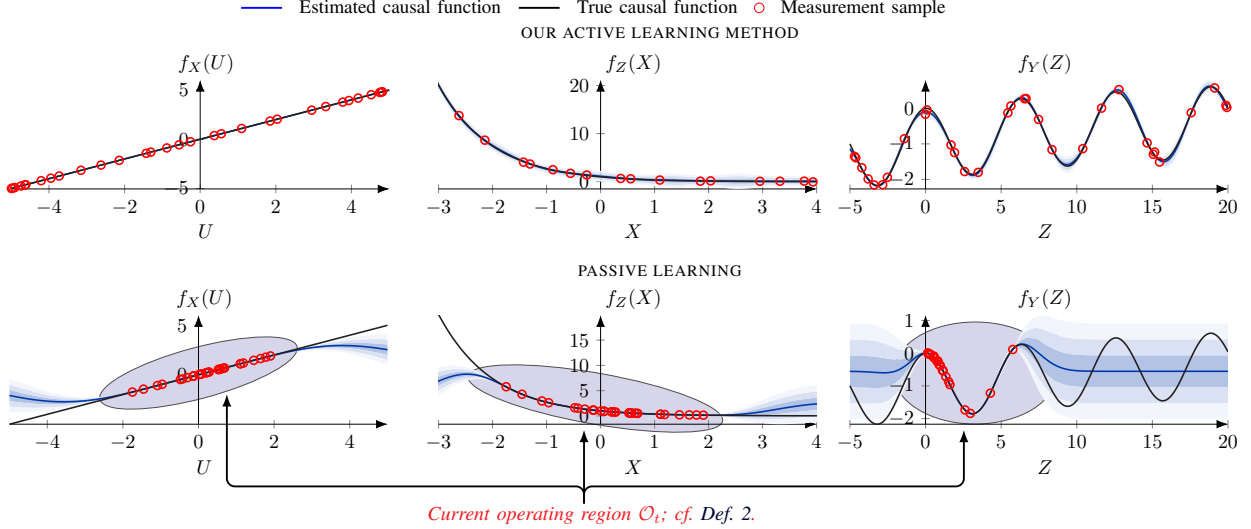


Fig. 5: Learned causal functions using the GP estimator $\varphi(\mathcal{D}_t)$ [cf. (6)] for the example SCM in §VI. The functions are learned based on 30 samples, i.e., $|\mathcal{D}_t| = 30$; cf. (3). The lower plots show the causal functions estimated through passive learning, i.e., the functions estimated from data collected through monitoring the system without influencing its operation through interventions. The upper plots show the functions estimated through our active learning method, i.e., the functions estimated from data collected using the rollout intervention policy; cf. (12). Curves show the mean values of the GPs; shaded regions indicate one, two, and three standard deviations from the mean (darker to lighter shades of blue).

where $\ell \geq 1$ is the lookahead horizon.

The benefit of this optimization is that it is guaranteed to yield an improved intervention policy (compared to the base policy) under general conditions, as stated below.

Proposition 3. *If the cost function g [cf. (9)] is bounded, the estimation in (11) is exact (i.e., $\bar{J}_\pi = J_\pi$), the operating region \mathcal{O} [cf. Def. 1] is a compact subset of a Euclidean space, and the function space \mathcal{F} [cf. (8)] is discretized such that the belief \mathbf{b} belongs to a compact subset of a Euclidean space, then the rollout policy $\tilde{\pi}$ obtained through (12) is guaranteed to improve the base policy π , i.e., $J_{\tilde{\pi}}(\mathbf{b}) \leq J_\pi(\mathbf{b})$ for all \mathbf{b} .*

Proposition 3 provides a performance guarantee for the rollout policy [cf. (12)] under certain conditions. It implies that the rollout policy will generally perform at least as well, and typically better than the base policy π . The proof follows directly from standard results by Bertsekas; see e.g., [16, Prop. 2.3.1], [21, Prop. 5.1.1], and [22, §2.4] for details.

From a computational point of view, the complexity of the minimization (12) can be adjusted according to available computing resources by tuning the lookahead horizon ℓ , the rollout horizon m , and the number of rollouts L . The main computational complexity stems from evaluating the expectations in (12) and (5). Fortunately, these expectations can be efficiently approximated via Monte-Carlo sampling.

VI. ILLUSTRATIVE EXAMPLE

To illustrate our method, we apply it to an SCM with the causal graph and functions shown in Fig. 6. The SCM is fixed over time and the causal functions are $\mathbf{F} = \{f_X, f_Z, f_Y\}$.

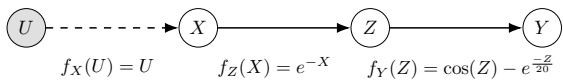


Fig. 6: The causal graph and functions of the SCM in the illustrative example.

Summary of our identification method (Fig. 4)

Our method for online identification of the causal model of an IT system includes the following steps. We assume we know the causal graph \mathcal{G} , which encodes the structural relationships within the IT system and which does not change over time. This graph defines a set of candidate models, each of which consists of a set of causal functions \mathbf{F}_t ; cf. (1). Starting at time $t = 1$ with initial dataset $\mathcal{D}_1 = \emptyset$, we repeat the following:

- 1) Estimate the causal functions \mathbf{F}_t [cf. (1)] based on the causal graph \mathcal{G} and the current dataset \mathcal{D}_t [cf. (3)] using the GP estimator $\varphi(\mathcal{D}_t)$; cf. (6).
- 2) Select the next intervention $\text{do}(\mathbf{X}'_t = \mathbf{x}'_t)$ using the rollout policy $\tilde{\pi}(\varphi(\mathcal{D}_t))$; cf. (12).
- 3) Perform the selected intervention, sample system measurements under the conditions imposed by the intervention according to (2), update the dataset \mathcal{D}_t [cf. (3)] to obtain \mathcal{D}_{t+1} , and restore the system to the settings before the intervention.

The SCM has four variables: one exogenous variable $\mathbf{U} = \{U\}$ and three endogenous variables $\mathbf{V} = \{X, Z, Y\}$. The exogenous variable U follows a Gaussian distribution, $U \sim \mathcal{N}(0, 0.1)$. The operating region [cf. Def. 1] is given by

$$\mathcal{R}(X) = \mathcal{R}(Y) = [-5, 5], \quad \mathcal{R}(Z) = [-5, 20], \quad \mathcal{R}(U) = [-\infty, \infty].$$

The measurement distributions (2) can be sampled with additive Gaussian noise $\alpha \sim \mathcal{N}(0, 0.05)$. All variables are controllable (i.e., $\mathbf{X} = \mathbf{V} \cup \mathbf{U}$) and the cost of each intervention except the passive intervention $\text{do}(\emptyset)$ is 1; cf. (9).

Instantiation of our method. We collect $M = 1$ samples per intervention. We define the cost approximation in (11)

as $\tilde{J}(\mathbf{b}) = \mathcal{L}(\mathbf{b})$; cf. (9). We configure the base policy π [cf. (12)] to always select the passive intervention $\text{do}(\emptyset)$. We set the lookahead and rollout horizons in (11)–(12) as $\ell = 1$ and $m = 5$, respectively. Finally, we define all GPs [cf. (6)] to have mean and covariance functions defined as

$$\begin{aligned} m(\mathbf{x}) &\triangleq 0, \\ k(\mathbf{x}, \mathbf{x}') &\triangleq \left(1 + \sqrt{5}r + \frac{5r^2}{3}\right) \exp\left(-\sqrt{5}r\right), \end{aligned} \quad (13)$$

for all input vectors \mathbf{x} and \mathbf{x}' , where $r \triangleq \|\mathbf{x} - \mathbf{x}'\|_2$ and $\|\cdot\|_2$ denotes the Euclidean norm. This covariance function encodes the assumption that the causal functions vary smoothly over the input space. Similarly, the mean function reflects the absence of prior knowledge of the function values. Further details about our experimental setup can be found in Appendix C.

Note that a broad variety of mean and covariance functions can be used to instantiate the GP estimator [cf. (6)]; see textbook [13] for details. Their design and parameterization offer a principled way to incorporate domain knowledge and structure (e.g., expected smoothness of the causal functions).

Baseline method. We compare the performance of our method with that of a baseline method that uses the same GP estimator [cf. (6)] but monitors the system without interventions. In other words, it uses the intervention policy $\pi(\mathbf{b}) = \text{do}(\emptyset)$ for all beliefs \mathbf{b} . We refer to this baseline as `PASSIVE LEARNING`.

Evaluation results. Figure 5 shows the causal functions estimated based on 30 samples collected through our active learning method and through passive learning. We observe that our method (upper plots) yields more accurate estimates of the true causal functions compared to passive learning (lower plots), especially for the nonlinear functions $f_Z(X)$ and $f_Y(Z)$. In particular, the GP posterior (blue curves) obtained through our method [cf. (6)] closely follows the causal functions (black lines) with low uncertainty (narrow shaded regions). In contrast, the GPs estimated through passive learning deviate significantly from the causal functions, particularly outside the system’s current operating region [cf. Def. 2], i.e., configurations of the system variables (X, Z, Y) that occur with low probability under the distribution $\mathbb{P}[U]$.

Figure 7 shows the value of the loss function \mathcal{L} [cf. (5)], which we approximate through discretization. We observe that as the number of samples $|\mathcal{D}_t|$ increases, the loss of the model estimated through our method (red curve) decreases rapidly. In contrast, the loss of the model estimated through passive learning (blue curve) decreases only slightly (from around 2400 to 2340), which is difficult to discern in the figure.

Table 1 compares the performance of different configurations of the rollout method; cf. (11)–(12). We find that rollout leads to a significant performance improvement when using a lookahead horizon of $\ell = 1$ and a rollout horizon of $m = 5$. This configuration amounts to around 12 seconds of computation with our commodity hardware (M4 PRO). Further increasing these horizons yields marginal improvements in performance while substantially increasing computation time.

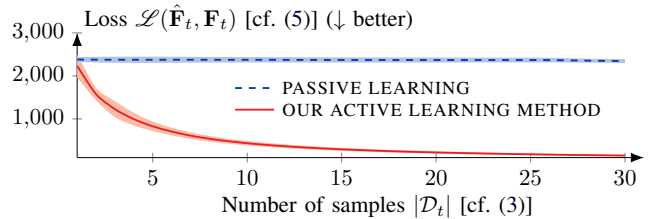


Fig. 7: Loss [cf. (5)] of the functions $\hat{\mathbf{F}}_t$ estimated through passive learning (blue curve) and our active learning method (red curve) for the example SCM in §VI. Curves show the mean value from evaluations with 5 random seeds; shaded areas indicate standard deviations.

Lookahead ℓ	Rollout m	Loss \mathcal{L} (\downarrow better)	Compute time (s)
-	-	2345	0.9
1	5	147	12.5
1	20	147	17.2
2	5	143	47.6
2	20	143	71.4
3	5	142	94.1
3	20	142	315.8

TABLE 1: Performance comparison of different instantiations of the rollout method [cf. (11)–(12)] based on the example SCM in §VI with $|\mathcal{D}_t| = 30$ samples; cf. (3). The performance is quantified by the loss function \mathcal{L} [cf. (5)] and the compute time to select each intervention. The first row contains the performance of the base policy π , which is defined as the policy that always selects the passive intervention $\text{do}(\emptyset)$, i.e., the policy of monitoring the system without interventions. We approximate the minimization (12) using Differential evolution (DE) [23, Fig. 3]; see Appendix C for details.

VII. IDENTIFYING A CAUSAL MODEL OF AN IT SYSTEM

In this section, we demonstrate how our method can be applied to identify a causal model of an IT system. We begin by describing the system configuration and our testbed implementation. Next, we outline the experimental setup and describe how we applied our method to identify the system. Lastly, we present and discuss the experimental findings.

A. IT System

We consider an IT system that involves a cloud-based web application with a backend composed of a web server and a service mesh. Services provided by this mesh are accessed by clients through a cloud gateway; see Fig. 8. The web server is implemented using `FLASK` [24] and the service mesh is implemented using `KUBERNETES` [25] and `ISTIO` [26].

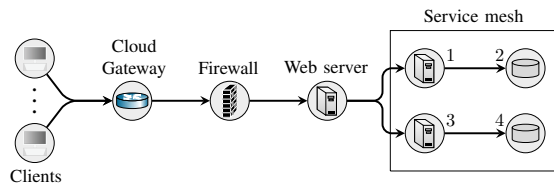


Fig. 8: Architecture of the IT system for the experimental evaluation: a cloud-based web application with a service mesh backend.

System configuration. The service mesh consists of 4 physical nodes (labeled 1–4 in Fig. 8), each of which runs two microservices. Specifically, nodes 1 and 3 run microservices (M_1, M_2) and nodes 2 and 4 run the microservice M_3 ; see

Table 2. Each node is implemented as a KUBERNETES pod, in which microservices execute within virtual containers.

Microservice	Description
Web application	A FLASK web application [24].
M_1	A web service that implements an electronic bookstore.
M_2	A CPU-intensive compute service for data processing.
M_3	MONGODB database [27].

TABLE 2: Configurations of microservices in the service mesh.

Network services. We deploy two services on the service mesh: an information service and a compute service, which we denote by S_1 and S_2 , respectively. Service S_1 invokes the microservices (M_1, M_3) and service S_2 invokes microservice M_2 . These services are accessed by clients that generate service requests, each of which can be handled in two ways, corresponding to different traversals of the service graph in Fig. 9. Specifically, a request for service S_1 can either traverse the subgraph FRONT NODE \rightarrow 1 \rightarrow 2 or traverse the subgraph FRONT NODE \rightarrow 3 \rightarrow 4. Similarly, a request for service S_2 can be processed by either node 1 or 3.

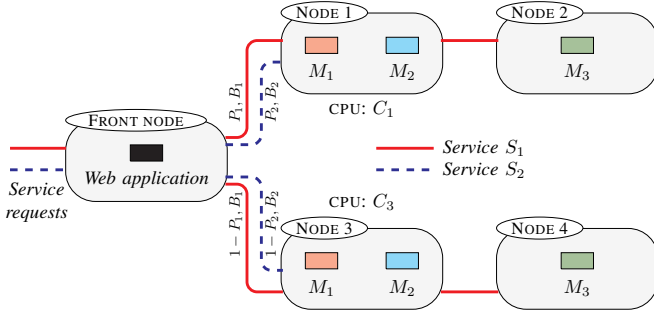


Fig. 9: Service mesh architecture of the IT system. Nodes are KUBERNETES pods running microservices M_i in containers, which collectively provide services S_1 and S_2 . Service S_1 invokes microservices $M_1 \rightarrow M_3$, and service S_2 invokes microservice M_2 . A request for service S_i is blocked with probability B_i . A service request can be routed via different subgraphs. The specific subgraph is selected probabilistically via P_i . All nodes have fixed resources except nodes 1 and 3, whose CPU counts (C_1, C_3) are scalable.

Request routing and blocking. The specific traversal path for a service request is decided by routing probabilities P_1 and P_2 , where P_i is the probability that a request for service S_i is routed to node 1. Apart from these probabilities, each request for service S_i is blocked at the front node with probability B_i .

Resource allocation. We denote by C_j the CPU allocation to node j in the service mesh; see Fig. 9. In our setup, the resource allocations are fixed for all nodes except for nodes 1 and 3, whose CPU counts (C_1 and C_3) are scalable.

Implementation. We run the IT system on our testbed at KTH. This testbed includes a cluster of POWEREDGE R715 2U servers connected through a gigabit Ethernet switch. Each server has 64 GB RAM, two 12-core AMD OPTERON processors, and four 1 GB network interfaces. All servers run UBUNTU SERVER 18.04.6 (64 bit) and their clocks are synchronized through the network time protocol [28]. The source code of our implementation and a dataset of traces from our testbed are available in [29].

B. Causal Model of the IT System

We model the system described in the preceding section as an SCM with the causal graph shown in Fig. 10. The system variables of the model are defined as follows.

- **Exogenous variables \mathbf{U} :**
 - B_i : blocking probability of service S_i ;
 - P_i : routing probability of service S_i to node 1;
 - C_j : CPU allocation to node j ;
 - L_i : load of service S_i (requests per second); and
 - $\epsilon_{R_1}, \epsilon_{R_2}$: random noise variables.
- **Endogenous variables \mathbf{V} :**
 - \tilde{L}_i : carried (i.e., non-blocked) load of service S_i ; and
 - R_i : response time (s) of service S_i .

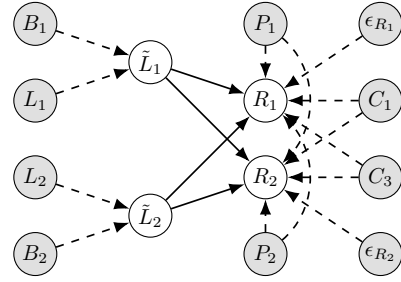


Fig. 10: Causal graph of the IT system in Fig. 8.

The operating region [cf. Def. 1] is defined as follows.

$$\begin{aligned} \mathcal{R}(B_i) &= \mathcal{R}(P_i) = [0, 1]; \quad \mathcal{R}(L_i) = \mathcal{R}(\tilde{L}_i) = [0, 50]; \\ \mathcal{R}(C_j) &= \{1, \dots, 5\}; \quad \mathcal{R}(\epsilon_{R_i}) = [-\infty, \infty]; \quad \mathcal{R}(R_i) = [0, 10]. \end{aligned}$$

All the exogenous variables except the noise variables are controllable, i.e.,

$$\mathbf{X} = \{B_1, B_2, L_1, L_2, P_1, P_2, C_1, C_3\}.$$

These variables can be externally controlled as follows: service loads (L_i) can be emulated; CPU allocations (C_j) can be configured in KUBERNETES; and the routing (P_i) and blocking probabilities (B_i) can be adjusted via ISTIO.

Following the graph in Fig. 10, the causal functions are

$$\tilde{L}_1 = f_{\tilde{L}_1, t}(B_1, L_1), \quad (14a)$$

$$\tilde{L}_2 = f_{\tilde{L}_2, t}(B_2, L_2), \quad (14b)$$

$$R_1 = f_{R_1, t}(\tilde{L}_1, \tilde{L}_2, P_1, P_2, C_1, C_3, \epsilon_{R_1}), \quad (14c)$$

$$R_2 = f_{R_2, t}(\tilde{L}_1, \tilde{L}_2, P_1, P_2, C_1, C_3, \epsilon_{R_2}). \quad (14d)$$

C. Evaluation Scenarios

To evaluate our method for identifying the causal functions in (14) from measurement data, we consider two scenarios: one focuses on identifying the functions during steady-state operation, and the other on tracking the causal functions as they change over time. In both scenarios, the system operates under a nominal configuration: the routing probabilities are set to $P_1 = P_2 = 0.5$, the CPU allocations to $C_1 = C_3 = 1$, and the blocking probabilities to $B_1 = B_2 = 0$. Interventions are required to change this configuration.



Fig. 11: Correlation matrix for the variables in the causal model [cf. Fig. 10] of the IT system in Fig. 8. The numbers in each cell indicate the Pearson correlation coefficient between two variables.

Scenario 1 (Stationary system). In this scenario, we run both the information service S_1 and the compute service S_2 on the service mesh. The service loads are kept constant with $L_1 = 4$ requests per second and $L_2 = 15$ requests per second. This setup defines the current operating region of the system; cf. Def. 2. The causal dependencies among the system variables follow the graph shown in Fig. 10.

Scenario 2 (Non-stationary system). In this scenario, we investigate how the estimates of the causal functions provided by our method adapt to a change in the service offering. The scenario is divided into two time intervals. In the first interval, which starts at $t = 1$, the service mesh runs only the compute service S_2 , which we load with $L_2 = 1$ requests per second. In the second interval, beginning at $t = 11$, we start the information service S_1 in the background and load it with $L_1 = 20$ requests per second. This change introduces additional background load on shared resources, such as CPU and bandwidth, which in turn affects the response time of service S_2 . As a result, the causal function for the response time, i.e., $f_{R_2,t}$, has to be re-estimated after the change.

To focus the analysis on the identification of the time-varying function $f_{R_2,t}$, we use a simplified SCM for this scenario. Specifically, we simplify the SCM for Scenario 1 by only considering variables related to service S_2 , i.e., we treat the influence of service S_1 as part of the environment. This simplification results in the causal graph shown in Fig. 13.

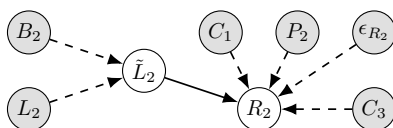


Fig. 13: Causal graph for Scenario 2.

D. Causal Functions

To evaluate our method, we need access to the causal functions \mathbf{F}_t [cf. (14)] to compute the loss function \mathcal{L} ; cf. (5). To obtain these functions, we explore the (complete) operating region [cf. Def. 1] and collect 100 samples per system variable for each configuration of control variables we consider. This (offline) process takes several days and yields a total dataset of over 30,000 measurement samples per system variable. We then use this data and the estimator φ [cf. (6)] to learn the causal functions \mathbf{F}_t . Figure 11 shows the correlation matrix of the collected data and Fig. 12 shows some of the causal functions. The matrix reveals several high correlations, not all of which are causal. For example, the load of service 1 (L_1) is correlated with the load of service 2 (L_2). Moreover, we observe in Fig. 12 that the causal functions model complex dependencies between the system variables.

E. Instantiation of Our Method

We apply our method to estimate the causal functions \mathbf{F}_t in Fig. 12. To this end, we instantiate our method as described in §VI, i.e., we define the base intervention policy in (12) to be the policy that always selects the passive intervention $\text{do}(\emptyset)$; we define the number of samples per intervention to be $M = 1$; we set the lookahead and rollout horizons in (11)–(12) as $\ell = 1$ and $m = 5$, respectively; we define the cost approximation in (11) as $\tilde{J}(\mathbf{b}) = \mathcal{L}(\mathbf{b})$; and we set the mean and covariance functions of the GP estimator φ [cf. (6)] according to (13). To allow the GP estimator to “forget” old data when the system changes in Scenario 2, we define the dataset \mathcal{D}_t [cf. (3)] as a first-in-first-out buffer of size 10.

Intervention costs. The cost function c [cf. (4)] depends on the operational impact of different interventions in a specific system. For our experiments, we define this function using the intervention costs listed in Table 3. These costs reflect the relative disruption of each intervention type, with high costs assigned to interventions like changing CPU allocations (C_j) and lower costs to less disruptive interventions, such as adjusting routing (R_i) or blocking (B_i) probabilities.

Intervention	Cost
Emulating the service load L_i	3000
Adjusting the routing probability P_i	1000
Adjusting the blocking probability B_i	2000
Modifying the CPU allocation C_j	3000
Monitoring without intervening, i.e., $\text{do}(\emptyset)$	1

TABLE 3: Intervention costs for defining the cost function c ; cf. (4).

F. Evaluation Results

The evaluation results for the two scenarios are detailed below. We present the results by visually comparing the estimated functions against the causal functions in Fig. 12 and showing how the loss \mathcal{L} [cf. (5)] evolves as additional measurement samples are collected.

Scenario 1 (Stationary system). Figure 14 shows the causal functions estimated using the GP estimator $\varphi(\mathcal{D}_t)$ [cf. (6)] based on 30 samples collected through passive learning. Because the data is collected without interventions, the data is

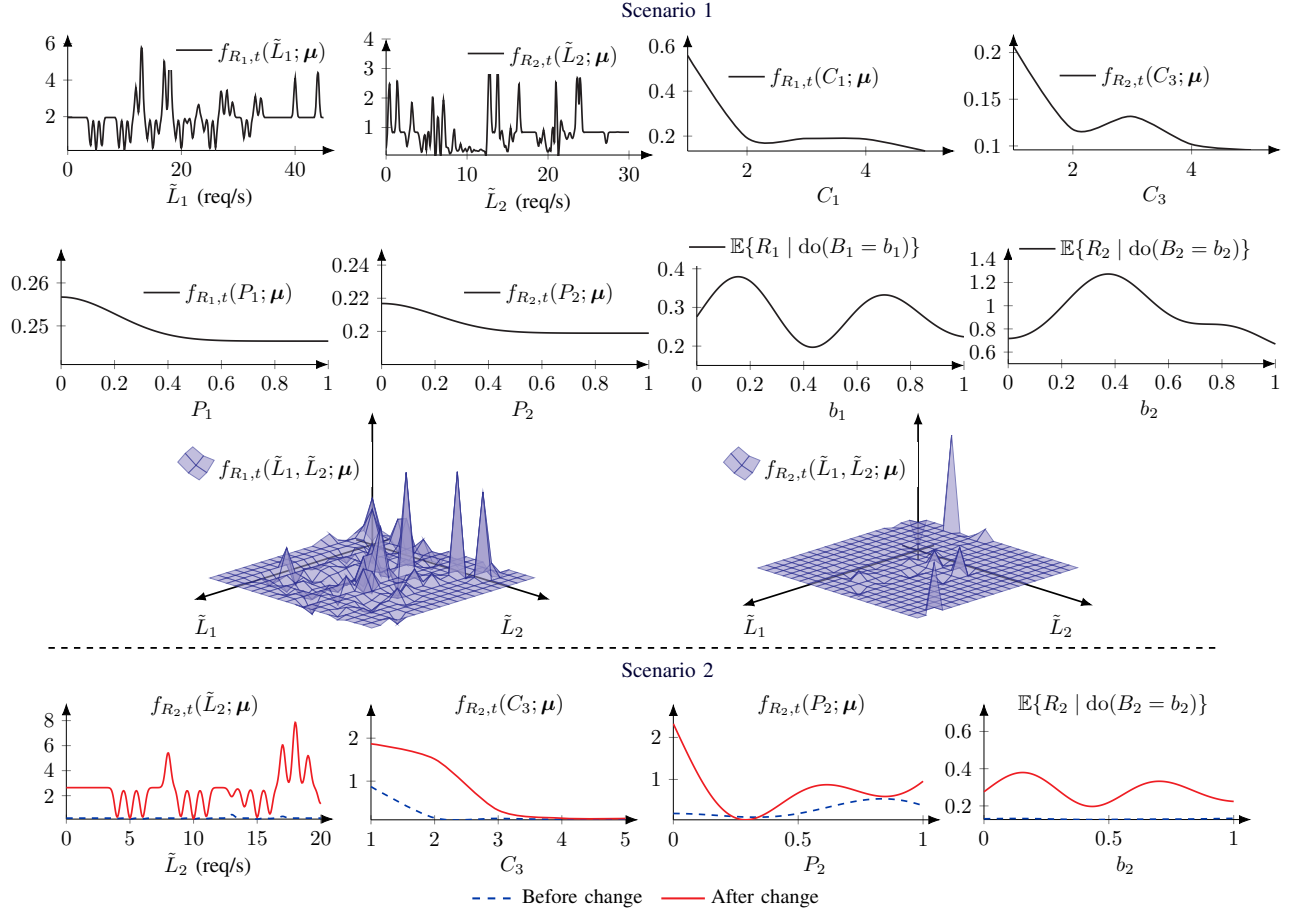


Fig. 12: Some of the causal functions in the structural causal model (SCM) of the IT system in Fig. 8. The function $f_{R_i,t}(\tilde{L}_i; \mu)$ denotes $f_{R_i,t}(\tilde{L}_1, \tilde{L}_2, P_1, P_2, C_1, C_3, \epsilon_{R_i})$ [cf. (14)] evaluated with all inputs fixed to their mean values except for \tilde{L}_i . The upper plots show the ground truth causal functions for Scenario 1 and the lower plots show the ground truth causal functions for Scenario 2.

confined to the system's *current* operating region; cf. Def. 2. As a result, the estimated causal functions exhibit high uncertainty in unexplored parts of the operating region; cf. Def. 1.

Figure 15 shows the causal functions estimated using the GP estimator $\varphi(\mathcal{D}_t)$ [cf. (6)] based on 30 samples collected with our active learning method, which uses the rollout intervention policy; cf. (12). Unlike the passive learning policy, this policy selects interventions that explore diverse configurations of the system, which enables our method to collect data outside of the current operating region; cf. Def. 2. As a result, the estimated functions better capture the system behavior.

Figure 16 shows the evolution of the causal effect $\mathbb{E}\{R_2 \mid \text{do}(B_2 = b_2)\}$ based on the causal functions estimated via our method. Initially, the estimate is uncertain due to a lack of data. However, as new samples are collected, the uncertainty rapidly shrinks and the estimate converges toward the true causal function, as expected from Prop. 1 and Prop. 2.

Lastly, Fig. 17 quantifies the accuracy of the estimated functions through the loss function \mathcal{L} ; cf. (5). We see in the figure that the loss of the functions estimated through passive learning plateaus and remains high. In contrast, the loss of the functions estimated through our active learning method reduces with each measurement sample. Specifically, the loss of passive learning (blue curve) decreases from around $2.8 \cdot 10^6$

to $2.77 \cdot 10^6$, which is negligible and barely visible in the plot. By comparison, the loss of our method decreases to $84 \cdot 10^3$.

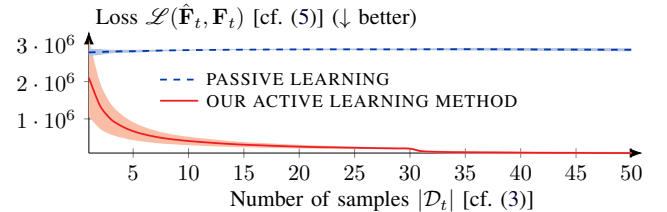


Fig. 17: Loss [cf. (5)] of the functions $\hat{\mathbf{F}}_t$ estimated through passive learning (blue curve) and our active learning method (red curve) when applied to Scenario 1. Curves show the mean value from evaluations with 5 random seeds; shaded areas indicate standard deviations.

Takeaway from Scenario 1.

Passive learning provides limited coverage of the system's operating region [cf. Def. 1], leading to inaccurate model estimates. Our active learning method overcomes this limitation by selecting interventions across the complete operating region.

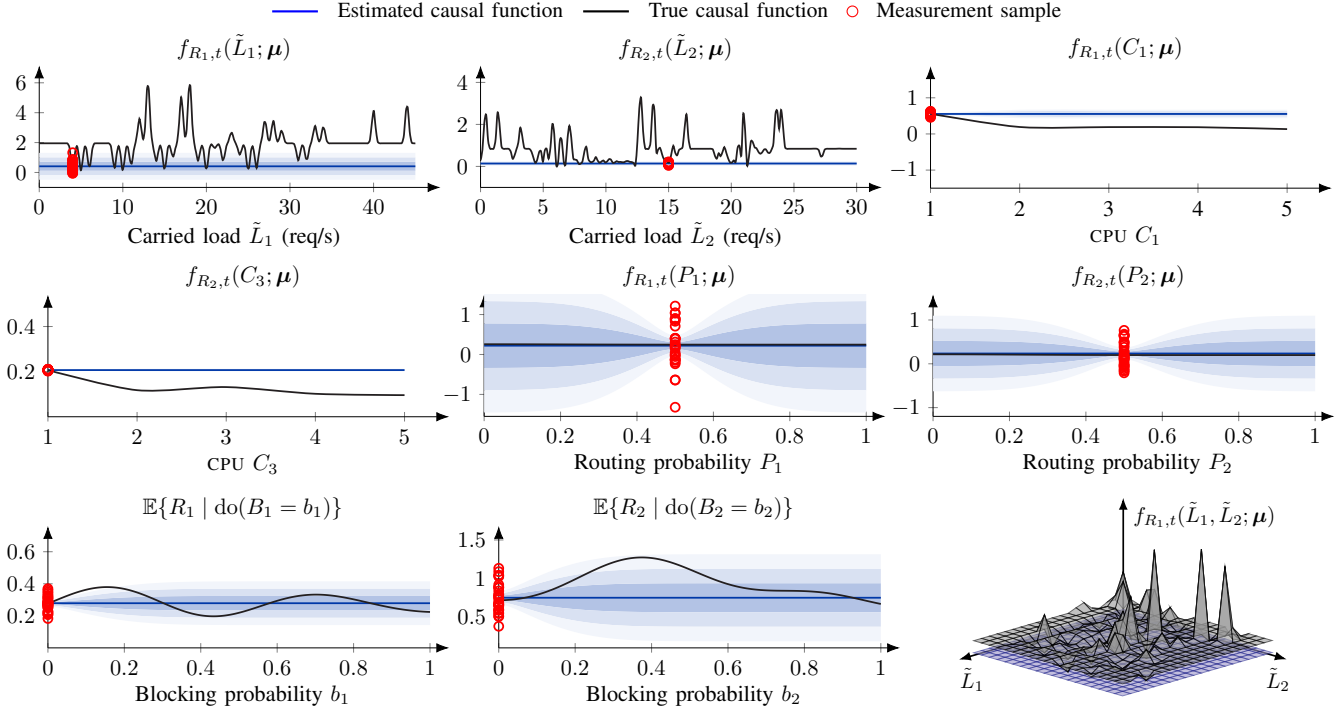


Fig. 14: Scenario 1: the system is stationary and the causal functions do not change. The figure shows some of the causal functions for the IT system described in §VII-A estimated using the GP estimator $\varphi(\mathcal{D}_t)$ [cf. (6)] based on 30 samples (i.e., $|\mathcal{D}_t| = 30$) collected through **passive learning**. Curves show the mean values; shaded regions indicate one, two, and three standard deviations from the mean (darker to lighter shades of blue). The function $f_{R_i,t}(\tilde{L}_1, \tilde{L}_2, P_1, P_2, C_1, C_3, \epsilon_{R_i})$ [cf. (14)] evaluated with all inputs fixed to their mean values except for \tilde{L}_i .

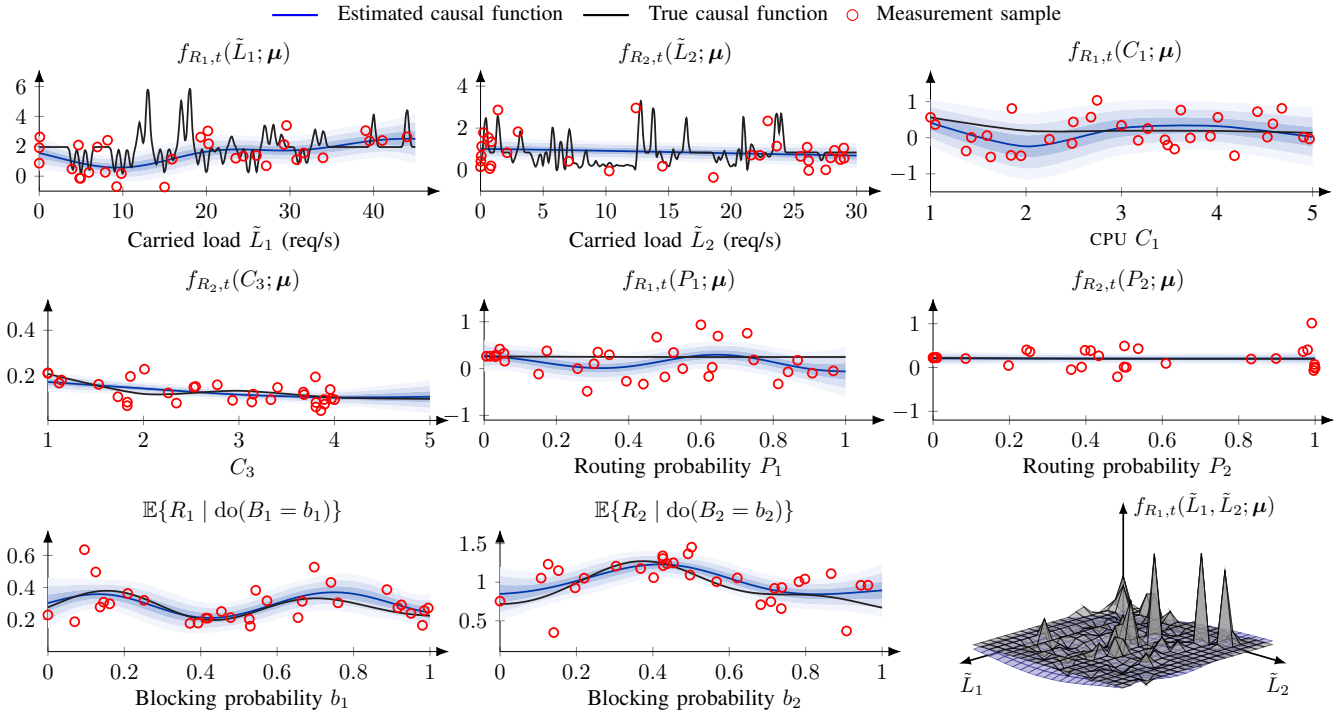


Fig. 15: Scenario 1: the system is stationary and the causal functions do not change. The figure shows learned causal functions for the IT system described in §VII-A. The functions are learned using the GP estimator $\varphi(\mathcal{D}_t)$ [cf. (6)] based on 30 samples (i.e., $|\mathcal{D}_t| = 30$) collected using our **active learning method** with the rollout intervention policy; cf. (12). Curves show the mean values; shaded regions indicate one, two, and three standard deviations from the mean (darker to lighter shades of blue). The function $f_{R_i,t}(\tilde{L}_i; \boldsymbol{\mu})$ denotes $f_{R_i,t}(\tilde{L}_1, \tilde{L}_2, P_1, P_2, C_1, C_3, \epsilon_{R_i})$ [cf. (14)] evaluated with all inputs fixed to their mean values except for \tilde{L}_i .

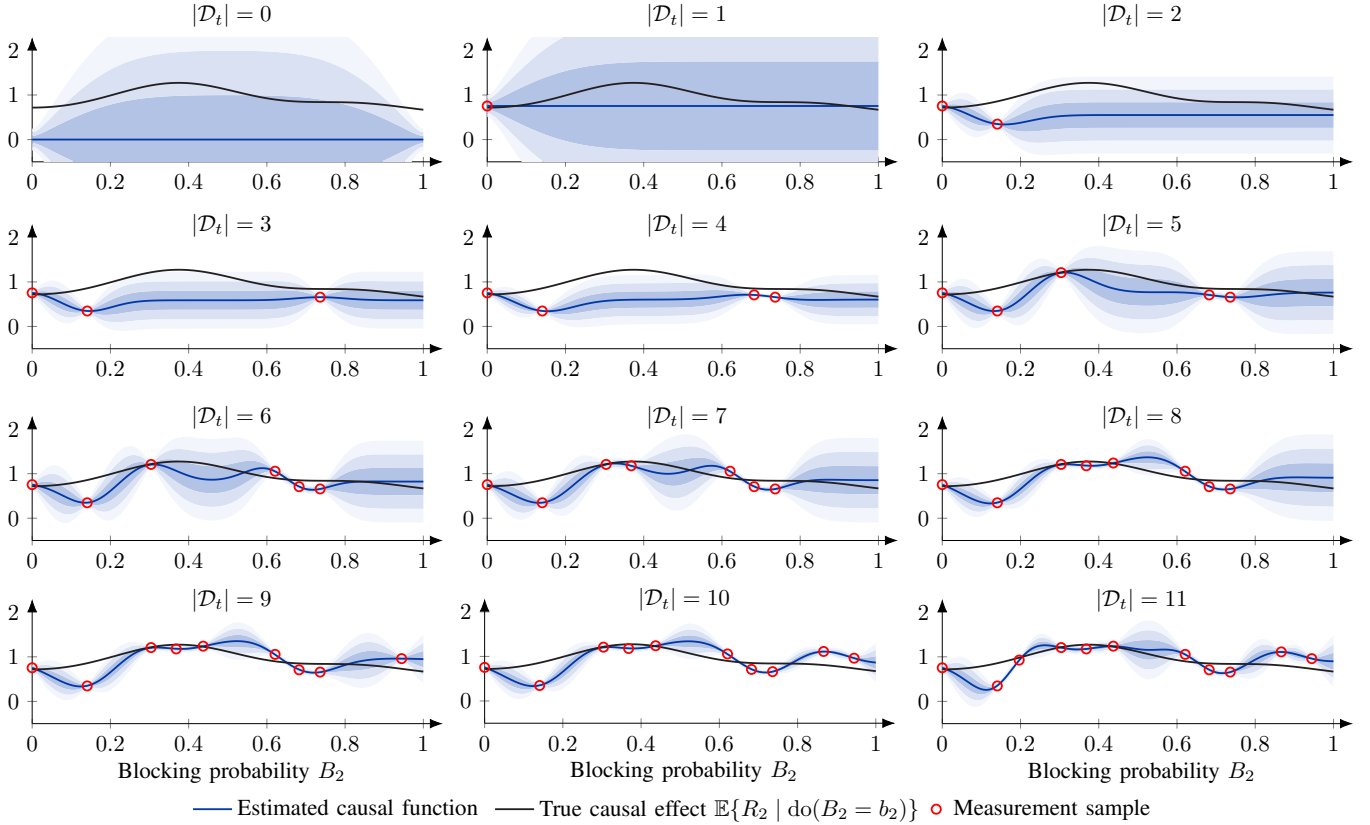


Fig. 16: Scenario 1: the system is stationary and the causal functions do not change. The figure shows the evolution of the causal effect $\mathbb{E}\{R_2 \mid \text{do}(B_2 = b_2)\}$ based on the functions \hat{F}_t estimated through (6) as the dataset \mathcal{D}_t [cf. (3)] is updated using our **active learning method** with the rollout intervention policy; cf. (12). Curves show the mean values; shaded regions indicate one, two, and three standard deviations from the mean (darker to lighter shades of blue).

Scenario 2 (Non-stationary system). Unlike Scenario 1, where the system is stationary, this scenario involves a change in the system between time steps $t = 10$ and $t = 11$. Figure 19 shows the model accuracy, as quantified by the loss function \mathcal{L} ; cf. (5). As in Scenario 1, we find that models estimated based on passive learning have persistently high loss. In contrast, the loss of the model estimated via our active learning method is steadily decreasing as more data is collected.

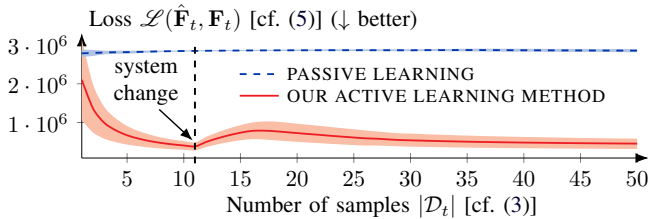


Fig. 19: Loss [cf. (5)] of the functions \hat{F}_t estimated through passive learning (blue curve) and our active learning method (red curve) when applied to Scenario 2. Curves show the mean value from evaluations with 5 random seeds; shaded areas indicate standard deviations.

At time step $t = 11$, the loss temporarily increases due to the system change. However, our method adapts by updating the model to reflect the new dynamics. Figure 18 illustrates this adaptation by showing how the estimate of the causal function $f_{R_2,t}$ [cf. (14)] evolves from $t = 10$ to $t = 21$. Initially, the estimate differs substantially from the true function, but by

$t = 21$, it closely aligns with the updated system behavior.

Takeaway from Scenario 2.

Unlike offline identification methods, which use a fixed dataset to estimate the model, our method estimates the model sequentially and selects interventions based on the uncertainty in the current estimate. This approach allows for quick adaptation of the model to system changes.

VIII. USE CASES OF THE IDENTIFIED CAUSAL MODEL

Once the causal functions F_t [cf. (1)] have been identified with sufficiently high confidence through our method, they can be used for optimizing various downstream tasks in IT systems. We give several examples of such use cases below.

Forecasting system metrics. The causal functions can be used to predict how key performance indicators evolve in response to changes in system variables, such as service loads and routing probabilities. For example, the function $f_{R_1,t}$ of the SCM in §VII predicts the response time of service S_1 based on the load, routing configuration, and CPU allocation.

Anomaly detection. The causal functions can be used to identify abnormal system behavior. For instance, in the context of the SCM described in §VII, if the response time R_i deviates

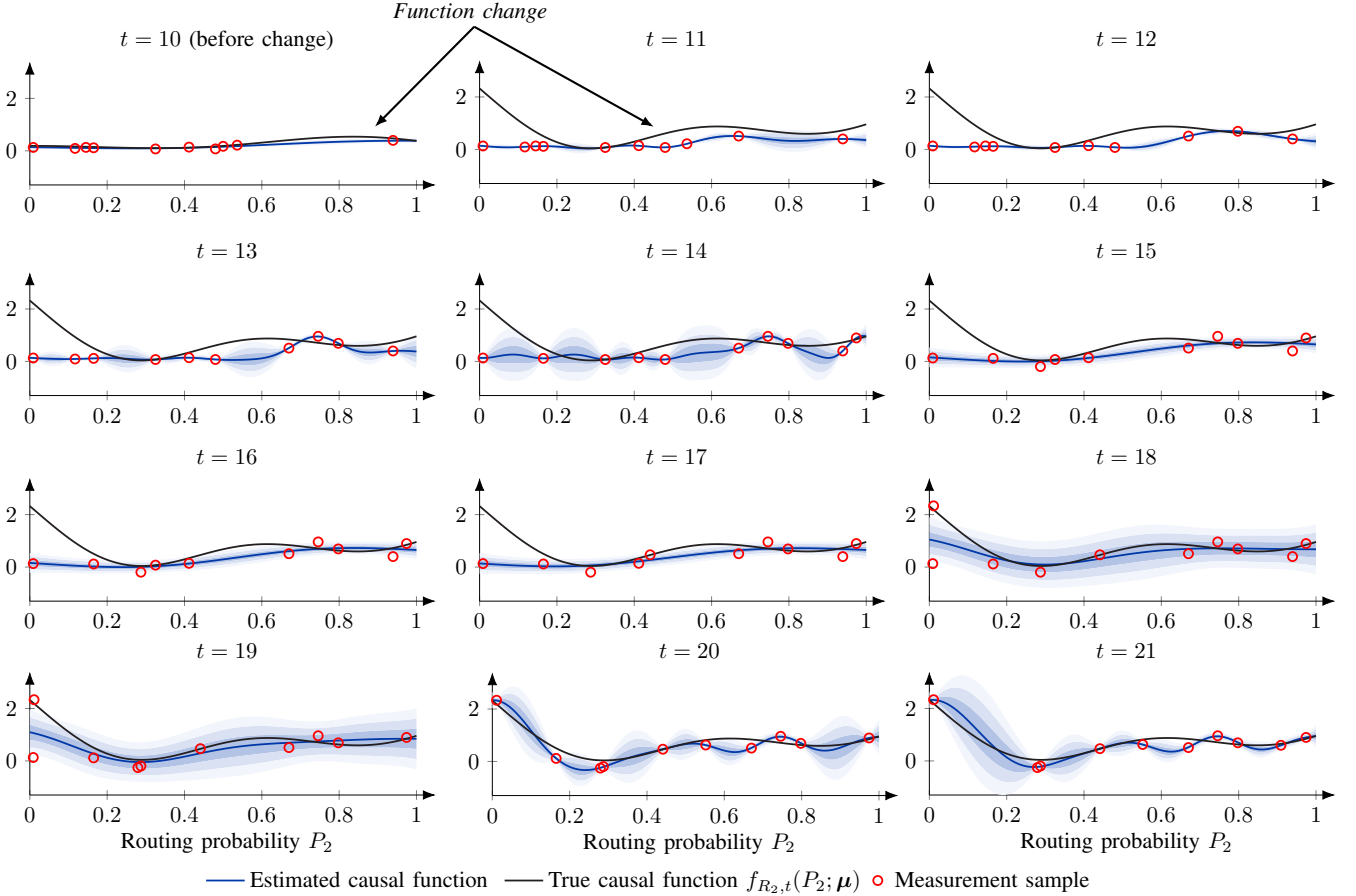


Fig. 18: Scenario 2: a change in the IT system occurs between time steps $t = 10$ and $t = 11$, which causes the function $f_{R_2,t}$ to change. The dataset \mathcal{D}_t [cf. (3)] is defined as a first-in-first-out buffer of size 10 and is updated using our **active learning method** with the rollout intervention policy; cf. (12). Curves show the mean values; shaded regions indicate one, two, and three standard deviations from the mean (darker to lighter shades of blue). The function $f_{R_2,t}(P_2; \mu)$ denotes $f_{R_2,t}(\bar{L}_1, \bar{L}_2, P_1, P_2, C_1, C_3, \epsilon_{R_i})$ [cf. (14)] evaluated with all inputs fixed to their mean values except for P_2 .

significantly from what the function $f_{R_i,t}$ predicts given the current load and configuration, this may indicate an ongoing performance anomaly or a potential cyberattack [30], [31].

Automatic control. The causal functions enable simulation-based optimization of control policies through reinforcement learning. For instance, the functions described in §VII define how varying the CPU counts C_1 and C_3 will affect the response times R_1 and R_2 . This cause-and-effect relationship can be used to optimize a resource allocation policy that dynamically scales C_1 and C_3 to keep the response times below a threshold.

Root cause analysis. The causal functions can support the diagnosis of system failures by tracing observed performance degradations or anomalies back to their causal origins.

Digital twin. The causal functions can be used to build a digital twin, i.e., a virtual replica of the IT system that provides a controlled environment for virtual operations [32], [33]. By using our method to periodically update the causal model based on new measurements, the digital twin can simulate the impact of hypothetical changes to the IT system (e.g., workload shifts, configuration updates, policy changes, or security interventions) before applying them to the IT system.

IX. DISCUSSION OF DESIGN CHOICES IN OUR METHOD

Our method involves two main steps: (i) estimation of causal functions through GP regression; and (ii) selection of interventions through rollout and lookahead optimization. The main reason for using GP regression is that it quantifies the uncertainty in its estimates, which we use to guide the selection of interventions. Alternatives to GP regression include mixture density networks (MDNs) [34] and Bayesian neural networks (BNNs) [35], both of which provide function estimates with uncertainty quantification. Compared to these methods, the main advantage of GPs is that they come with theoretical guarantees: under general conditions, they can approximate any continuous function arbitrarily well; see Prop. 2. By contrast, MDNs and BNNs typically require careful tuning of the neural network architecture to obtain accurate estimates.

On the other hand, MDNs and BNNs scale more favorably to large datasets than GPs. In particular, the computational complexity of GP regression is cubic in the size of the dataset [13]. However, this complexity can be addressed using sparse GP approximations [36] or neural GP methods [37], which reduce complexity while retaining most of the predictive accuracy. Another practical approach is to use a first-in-first-out buffer to bound the dataset size during online learning, as we did in the experiments related to Scenario 2.

In addition to MDNs and BNNS, another alternative to GPs is conformal prediction (also known as hedged prediction [38]), which can be applied on top of any function estimator to provide uncertainty quantification [39]. For instance, random forest regressors or feedforward neural networks can serve as base estimators for conformal prediction. Compared to GPs, these models may be easier to scale to large datasets, but they generally lack the convergence guarantees of GPs.

Regarding the selection of interventions, the main alternatives to our rollout method [cf. (12)] are random selection and heuristic selection. Examples of such methods include ϵ -greedy, Thompson sampling, upper-confidence-bound strategies, and myopic one-step lookahead policies; see textbook [40] for a comprehensive overview of these methods. Compared to these methods, the advantages of our rollout method are a) that it uses the GP’s uncertainty estimates to drive exploration of the system’s (complete) operating region [cf. Def. 1]; and b) that it is couched on well-established theory; see [16], [17]. (Note that the computation of an optimal intervention policy is intractable, which is why exact dynamic programming methods are not a viable alternative to rollout.)

X. RELATED WORK

System identification has a long history in the control systems community, where the primary goal is to build mathematical models of dynamic systems from observed input-output data [41]–[44]. In parallel, related ideas have been studied in the artificial intelligence (AI) and reinforcement learning communities, where the task is often referred to as model learning rather than system identification [45]–[47]. However, there are essential differences between these classical approaches and our method. First, most existing work in both control and AI focuses on physical or simulated control systems, whereas our emphasis is on modeling IT systems. Second, traditional methods are generally offline and assume access to large batches of data, while our approach is designed for online learning of a causal model. The benefit of our approach is that it allows to quickly adapt the model to system changes, such as service migrations or software updates.

Online system identification has received attention in the context of adaptive control and dual control. In this line of research, the goal is to design methods for simultaneously identifying an unknown dynamical system while controlling it [48]–[57]. Adaptive control typically identifies the system based on measurements from the current operating region, whereas dual control explicitly selects controls to explore the complete operating region. The main difference between these works and our paper is that we focus on learning a structural causal model, whereas the referenced works focus on learning a dynamical system model, such as a linear system [44] or a Markov decision process [48]. Moreover, our problem formulation is different. Our objective is to accurately learn the underlying (causal) system model from system measurements. By contrast, the objective in most of the referenced works is to simultaneously learn a system model and a control policy.

Online causal learning has been studied in the contexts of causal Bayesian optimization and causal discovery. In causal

Bayesian optimization, the objective is to identify interventions that maximize a target variable in a causal model with known structure but unknown dynamics [58]–[62]. While methods designed for such problems typically involve learning the causal functions, this is not the main goal. Rather, the main goal is to learn just enough about the causal functions to identify an optimal intervention. Causal discovery, on the other hand, seeks to learn the causal structure from data [63], [64]. This line of work differs from our paper in that we aim to learn the causal functions rather than the causal structure.

Prior work that focuses on the same problem as us includes [65]–[68] and [69]. Compared to these papers, the main difference is that our method is designed explicitly for IT systems, whereas the referenced papers focus on other types of systems, e.g., healthcare systems [67]. Moreover, our intervention policy is based on rollout, whereas the referenced papers use (myopic) heuristic intervention policies.

Lastly, we note that a growing body of research applies causal modeling to various decision-making problems that arise in the operation of IT systems, particularly in cybersecurity [70], [71] and root cause analysis [72]–[75]. However, these approaches assume the existence of a causal model and focus on specific decision-making tasks. In contrast, our method addresses the more general problem of learning the causal system model itself, which can then support a wide range of downstream tasks in IT systems.

XI. CONCLUSION

A longstanding goal in systems engineering and operation is to automate network and service management tasks. We argue that a key component to achieve such automation is a causal model that explains how changes to system variables affect system behavior. Traditionally, such models have been designed by domain experts, which does not scale with the growing complexity and increasing dynamism of IT systems.

This paper presents a method for online, data-driven identification of a causal system model. The main idea is to learn the system dynamics through *active causal learning*, where a rollout policy selects targeted interventions that generate data to update the model via Gaussian process regression. We show that this method is Bayes-optimal (Prop. 1), asymptotically consistent (Prop. 2), and that the intervention policy has the cost improvement property (Prop. 3). Testbed experiments demonstrate that our method quickly identifies accurate models of dynamic systems at a low operational cost.

Future work. From a practical point of view, an important direction for future work is to investigate further use cases of causal models identified through our method, such as real-time control, diagnosis, and forecasting in IT systems. We have not presented a thorough study of such tasks in this paper to keep the focus on presenting the core method.

From a theoretical perspective, a natural extension of this work is to generalize our method by relaxing certain assumptions. In particular, the current problem formulation assumes that the causal graph and the distribution of exogenous variables are fixed and known. The first assumption can be relaxed by incorporating causal discovery methods for identifying the

Notation(s)	Description
$\mathcal{M}_t, \mathcal{G}$	Structural causal model, causal graph; cf. (1).
$\mathbf{U}, \mathbf{V}, \mathbf{F}_t$	Exo/endo-genous variables and functions of SCM \mathcal{M}_t ; cf. (1).
\mathbf{X}, \mathbf{N}	Controllable/non-controllable variables of SCM \mathcal{M}_t ; cf. (1).
φ, π	Estimator [cf. (6)] and intervention policy; cf. (4).
$\mathcal{L}, \mathcal{D}_t$	Loss function [cf. (5)] and dataset [cf. (3)].
c, γ	Cost function and discount factor; cf. (4).
\mathcal{L}, g	Expected loss and cost functions; cf. (9).
ℓ, m	Rollout and lookahead horizons; cf. (12).
L	Number of rollouts cf. (11).
$\pi, \tilde{\pi}$	Base and rollout policies; cf. (12).
$\mathbf{b}_t, \mathbf{z}_t$	Belief state and measurement; cf. (7).
u_t	Rollout control (intervention) at time t ; cf. (7).
J_π	Cost-to-go function of the policy π ; cf. (10).
$\boldsymbol{\mu}, \boldsymbol{\Sigma}$	Mean vector and covariance matrix; cf. Appendix D.
$\mathcal{N}(\boldsymbol{\mu}, \boldsymbol{\Sigma})$	Multivariate Gaussian distribution; cf. Appendix D.
m_i, k_i	Mean and covariance functions of a Gaussian process; cf. §V-A.
$r \sim \mathcal{GP}(m_i, k_i)$	Sampling a function r from a Gaussian process; cf. §V-A.
$\mathcal{GP}(m_i, k_i)$	Posterior Gaussian process after observing \mathcal{D} ; cf. §V-A.
$\text{do}(\mathbf{X} = \mathbf{x})$	Intervention assigning the values \mathbf{x} to the variables in \mathbf{X} ; cf. §IV.
$\text{do}(\emptyset)$	The passive intervention; cf. §IV.
M	The number of samples obtained after an intervention; cf. §IV.
\mathcal{O}	The (complete) operating region; cf. Def. 1.
\mathcal{O}_t	The current operating region; cf. Def. 2.

TABLE 4: Notation.

graph from data. The second assumption is purely for ease of exposition; removing it has minimal effect on implementation and theory. In particular, if the distribution of exogenous variables is unknown and time varying, it can be learned with the same method we use for learning the causal functions. The only notable change is that the loss function \mathcal{L} [cf. (5)] and the surrogate loss function \mathcal{L} [cf. (8)] must be updated to include a term that quantifies the accuracy of the estimated distribution, e.g., based on the Kullback-Leibler divergence.

ACKNOWLEDGMENTS

This research is supported by the Swedish Research Council under contract 2024-06436. The authors would like to thank Forough Shahab Samani for her help in setting up the testbed.

APPENDIX A NOTATION

Our notation is summarized in Table 4.

APPENDIX B PROOF OF PROPOSITION 1

For ease of notation we write $\hat{\mathbf{F}}, f_{V_i}, \mathbf{F}, \hat{f}_{V_i}$ instead of $\hat{\mathbf{F}}_t, f_{V_i,t}, \mathbf{F}_t, \hat{f}_{V_i,t}$. Moreover, we write \mathbf{x} instead of \mathbf{x}_i . We seek to find the estimator $\hat{\mathbf{F}}$ that minimizes the expected loss $\mathbb{E}_{\mathbf{F} \sim \varphi(\mathcal{D}_t)} \{\mathcal{L}(\hat{\mathbf{F}}, \mathbf{F})\}$. We start by expanding this loss using the definition of \mathcal{L} [cf. (5)], which gives

$$\begin{aligned}
& \mathbb{E}_{\mathbf{F} \sim \varphi(\mathcal{D}_t)} \{\mathcal{L}(\hat{\mathbf{F}}, \mathbf{F})\} \\
&= \mathbb{E}_{\mathbf{F} \sim \varphi(\mathcal{D}_t)} \left\{ \sum_{V_i \in \mathbf{V}} \int_{\mathcal{R}(\text{pa}_{\mathcal{G}}(V_i))} \left(f_{V_i}(\mathbf{x}) - \hat{f}_{V_i}(\mathbf{x}) \right)^2 \mathbb{P}[\text{d}\mathbf{x}] \right\} \\
&= \sum_{V_i \in \mathbf{V}} \int_{\mathcal{R}(\text{pa}_{\mathcal{G}}(V_i))} \mathbb{E}_{\mathbf{F} \sim \varphi(\mathcal{D}_t)} \left\{ \left(f_{V_i}(\mathbf{x}) - \hat{f}_{V_i}(\mathbf{x}) \right)^2 \right\} \mathbb{P}[\text{d}\mathbf{x}] \\
&= \sum_{V_i \in \mathbf{V}} \int_{\mathcal{R}(\text{pa}_{\mathcal{G}}(V_i))} \mathbb{E}_{f_{V_i} \sim \mathcal{GP}(m_i, k_i)} \left\{ \left(f_{V_i}(\mathbf{x}) - \hat{f}_{V_i}(\mathbf{x}) \right)^2 \right\} \mathbb{P}[\text{d}\mathbf{x}].
\end{aligned}$$

Applying standard GP properties, we decompose $f_{V_i} | \mathcal{D}_t$ as

$$(f_{V_i} | \mathcal{D}_t)(\mathbf{x}) = m_i | \mathcal{D}_t(\mathbf{x}) + h_i(\mathbf{x}) \quad \text{for all } \mathbf{x} \text{ and } V_i,$$

where $h_i \sim \mathcal{GP}(m_0, k_i | \mathcal{D}_t)$ and $m_0(\mathbf{x}) = 0$ for all \mathbf{x} . Leveraging this decomposition, we can rewrite the loss as

$$\begin{aligned}
& \mathbb{E}_{\mathbf{F} \sim \varphi(\mathcal{D}_t)} \{\mathcal{L}(\hat{\mathbf{F}}, \mathbf{F})\} = \sum_{V_i \in \mathbf{V}} \int_{\mathcal{R}(\text{pa}_{\mathcal{G}}(V_i))} \left(\mathbb{E}_{h_i \sim \mathcal{GP}(m_0, k_i | \mathcal{D}_t)} \left\{ \left(m_i | \mathcal{D}_t(\mathbf{x}) + h_i(\mathbf{x}) - \hat{f}_{V_i}(\mathbf{x}) \right)^2 \right\} \right) \mathbb{P}[\text{d}\mathbf{x}] \\
&= \sum_{V_i \in \mathbf{V}} \int_{\mathcal{R}(\text{pa}_{\mathcal{G}}(V_i))} \mathbb{E}_{h_i \sim \mathcal{GP}(m_0, k_i | \mathcal{D}_t)} \left\{ \left(m_i | \mathcal{D}_t(\mathbf{x}) - \hat{f}_{V_i}(\mathbf{x}) \right)^2 \right. \\
&\quad \left. + 2h_i(\mathbf{x}) \left(m_i | \mathcal{D}_t(\mathbf{x}) - \hat{f}_{V_i}(\mathbf{x}) \right) + (h_i(\mathbf{x}))^2 \right\} \mathbb{P}[\text{d}\mathbf{x}] \\
&= \sum_{V_i \in \mathbf{V}} \int_{\mathcal{R}(\text{pa}_{\mathcal{G}}(V_i))} \left(\left(m_i | \mathcal{D}_t(\mathbf{x}) - \hat{f}_{V_i}(\mathbf{x}) \right)^2 \right. \\
&\quad \left. + 2\mathbb{E}_{h_i \sim \mathcal{GP}(m_0, k_i | \mathcal{D}_t)} \{h_i(\mathbf{x})\} \left(m_i | \mathcal{D}_t(\mathbf{x}) - \hat{f}_{V_i}(\mathbf{x}) \right) + \mathbb{E}_{h_i \sim \mathcal{GP}(m_0, k_i | \mathcal{D}_t)} \left\{ (h_i(\mathbf{x}))^2 \right\} \right) \mathbb{P}[\text{d}\mathbf{x}] \\
&= \sum_{V_i \in \mathbf{V}} \int_{\mathcal{R}(\text{pa}_{\mathcal{G}}(V_i))} \left(\left(m_i | \mathcal{D}_t(\mathbf{x}) - \hat{f}_{V_i}(\mathbf{x}) \right)^2 \right. \\
&\quad \left. + k_i | \mathcal{D}_t(\mathbf{x}, \mathbf{x}) \right) \mathbb{P}[\text{d}\mathbf{x}].
\end{aligned}$$

Clearly, the minimizer of this expression is obtained by setting $\hat{f}_{V_i} = m_i | \mathcal{D}_t(\mathbf{x})$ for all V_i and \mathbf{x} . As a consequence, we have

$$\mathbb{E}_{\mathbf{F} \sim \varphi(\mathcal{D}_t)} \{\mathbf{F}\} \in \arg \min_{\hat{\mathbf{F}}} \mathbb{E}_{\mathbf{F} \sim \varphi(\mathcal{D}_t)} \left\{ \mathcal{L}(\hat{\mathbf{F}}, \mathbf{F}) \right\}.$$

□

APPENDIX C EXPERIMENTAL SETUP

All computations are performed using an M4 PRO chip. We approximate the integrals in (9) using 100 Monte-Carlo samples. The hyperparameters we use for the evaluation are listed in Table 5 and are selected based on random search.

Parameter	Value
Monte-carlo samples L [cf. (11)]	10
Minimizer of (12)	Differential evolution (DE) [23, Fig. 3]
Population size of DE	10
Iterations of DE	30

TABLE 5: Hyperparameters.

APPENDIX D GAUSSIAN PROCESS FORMULAS

A Gaussian process (GP) is a collection of random variables, any finite number of which have a joint Gaussian distribution; see [13, Def. 2.1] for a formal definition. It generalizes the Gaussian distribution and is specified by its mean function $m(\mathbf{x})$ and covariance function $k(\mathbf{x}, \mathbf{x}')$. Suppose that we want to estimate the output of the causal function $f_{V_i,t} \in \mathbf{F}_t$

[cf. (1)] at inputs $\mathbf{x}_* \triangleq (\mathbf{x}_1, \dots, \mathbf{x}_n)$. The mean and covariance functions can be used to define the Gaussian distribution $\mathbf{f}_* \triangleq (f_{V_{i,t}}(\mathbf{x}_1), \dots, f_{V_{i,t}}(\mathbf{x}_n)) \sim \mathcal{N}(\boldsymbol{\mu}, \boldsymbol{\Sigma})$, where $\boldsymbol{\mu} \triangleq (m(\mathbf{x}_1), \dots, m(\mathbf{x}_n))$ and

$$\boldsymbol{\Sigma} \triangleq K(\mathbf{x}_*, \mathbf{x}_*) \triangleq \begin{bmatrix} k(\mathbf{x}_1, \mathbf{x}_1) & k(\mathbf{x}_1, \mathbf{x}_2) & \cdots & k(\mathbf{x}_1, \mathbf{x}_n) \\ k(\mathbf{x}_2, \mathbf{x}_1) & k(\mathbf{x}_2, \mathbf{x}_2) & \cdots & k(\mathbf{x}_2, \mathbf{x}_n) \\ \vdots & \vdots & \ddots & \vdots \\ k(\mathbf{x}_n, \mathbf{x}_1) & k(\mathbf{x}_n, \mathbf{x}_2) & \cdots & k(\mathbf{x}_n, \mathbf{x}_n) \end{bmatrix}.$$

Since this Gaussian construction is feasible for an arbitrary (finite) number of input values n , the GP effectively defines a probability distribution over functions. We denote this distribution as $f_{V_{i,t}} \sim \mathcal{GP}(m, k)$.

Suppose that we observe the function values $\hat{\mathbf{f}} \triangleq (f_{V_{i,t}}(\hat{\mathbf{x}}_1) + \epsilon_1, \dots, f_{V_{i,t}}(\hat{\mathbf{x}}_M) + \epsilon_M)$ and the inputs $\hat{\mathbf{x}} \triangleq (\hat{\mathbf{x}}_1, \dots, \hat{\mathbf{x}}_M)$, where each ϵ_i is an i.i.d. Gaussian noise term with variance σ_ϵ^2 . Let $\mathcal{D}_t = \{\hat{\mathbf{f}}, \hat{\mathbf{x}}\}$ denote the dataset of these samples. We can then construct the posterior Gaussian distribution $\mathbb{P}[\mathbf{f}_* | \mathcal{D}_t] = \mathcal{N}(\boldsymbol{\mu}_{\mathcal{D}_t}, \boldsymbol{\Sigma}_{\mathcal{D}_t})$ via the calculations

$$\begin{aligned} \boldsymbol{\mu}_{\mathcal{D}_t} &= \mathbb{E}[\mathbf{f}_* | \mathbf{x}_*, \hat{\mathbf{f}}, \hat{\mathbf{x}}] \\ &= m(\mathbf{x}_*) + K(\mathbf{x}_*, \hat{\mathbf{x}})(K(\hat{\mathbf{x}}, \hat{\mathbf{x}}) + \sigma_\epsilon^2 \mathbf{I}_M)^{-1}(\hat{\mathbf{f}} - m(\hat{\mathbf{x}})), \\ \boldsymbol{\Sigma}_{\mathcal{D}_t} &= K(\mathbf{x}_*, \mathbf{x}_*) - K(\mathbf{x}_*, \hat{\mathbf{x}})(K(\hat{\mathbf{x}}, \hat{\mathbf{x}}) + \sigma_\epsilon^2 \mathbf{I}_M)^{-1}K(\hat{\mathbf{x}}, \mathbf{x}_*), \end{aligned}$$

where \mathbf{I}_M is the $M \times M$ identity matrix and $m(\hat{\mathbf{x}})$ is a shorthand for $(m(\hat{\mathbf{x}}_1), \dots, m(\hat{\mathbf{x}}_M))$ [13].

This posterior allows us to predict $f_{V_{i,t}}(\mathbf{x}_j)$ using the mean $(\boldsymbol{\mu}_{\mathcal{D}_t})_j$, whose uncertainty is quantified by the variance $(\boldsymbol{\Sigma}_{\mathcal{D}_t})_{jj}$. Since we can make such predictions for any input \mathbf{x}_j , the posterior is also a GP, which we denote as

$$f_{V_{i,t}} | \mathcal{D}_t \sim \mathcal{GP}(m_{|\mathcal{D}_t}, k_{|\mathcal{D}_t}).$$

Here $m_{|\mathcal{D}_t}(\mathbf{x})$ and $k_{|\mathcal{D}_t}(\mathbf{x}, \mathbf{x}')$ denote the posterior mean and covariance functions given the dataset $\mathcal{D}_t = \{\hat{\mathbf{f}}, \hat{\mathbf{x}}\}$, i.e.,

$$\begin{aligned} m_{|\mathcal{D}_t}(\mathbf{x}) &\triangleq m(\mathbf{x}) + k(\mathbf{x}, \hat{\mathbf{x}})(K(\hat{\mathbf{x}}, \hat{\mathbf{x}}) + \sigma_\epsilon^2 \mathbf{I}_M)^{-1}(\hat{\mathbf{f}} - m(\hat{\mathbf{x}})), \\ k_{|\mathcal{D}_t}(\mathbf{x}, \mathbf{x}') &\triangleq k(\mathbf{x}, \mathbf{x}') - k(\mathbf{x}, \hat{\mathbf{x}})(K(\hat{\mathbf{x}}, \hat{\mathbf{x}}) + \sigma_\epsilon^2 \mathbf{I}_M)^{-1}k(\hat{\mathbf{x}}, \mathbf{x}'). \end{aligned}$$

Here, $k(\mathbf{x}, \hat{\mathbf{x}})$ is a shorthand for the vector $(k(\mathbf{x}, \hat{\mathbf{x}}_1), \dots, k(\mathbf{x}, \hat{\mathbf{x}}_M))$.

REFERENCES

- [1] M. Sloman, "Policy driven management for distributed systems," *Journal of Network and Systems Management*, vol. 2, no. 4, pp. 333–360, 1994.
- [2] J. O. Kephart and D. M. Chess, "The vision of autonomic computing," *Computer*, vol. 36, no. 1, pp. 41–50, 2003.
- [3] C. Prehofer and C. Bettstetter, "Self-organization in communication networks: principles and design paradigms," *IEEE Communications magazine*, vol. 43, no. 7, pp. 78–85, 2005.
- [4] A. Clemm, L. Ciavaglia, L. Z. Granville, and J. Tantsura, "RFC 9315: Intent-based networking-concepts and definitions," 2022.
- [5] C. Grasso, R. Raftopoulos, and G. Schembra, "Smart zero-touch management of UAV-based edge network," *IEEE Transactions on Network and Service Management*, vol. 19, no. 4, pp. 4350–4368, 2022.
- [6] E. Coronado, R. Behravesht, T. Subramanya, A. Fernandez-Fernandez, M. S. Siddiqui, X. Costa-Pérez, and R. Riggio, "Zero touch management: A survey of network automation solutions for 5G and 6G networks," *IEEE Communications Surveys & Tutorials*, vol. 24, no. 4, pp. 2535–2578, 2022.
- [7] J. Pearl, *Causality: models, reasoning and inference*. Cambridge university press, 2009.
- [8] I. Shpitser and J. Pearl, "Complete identification methods for the causal hierarchy," *Journal of Machine Learning Research*, vol. 9, no. 9, 2008.
- [9] J. Peters, D. Janzing, and B. Schölkopf, *Elements of causal inference: foundations and learning algorithms*. The MIT press, 2017.
- [10] J. L. Hellerstein, Y. Diao, S. Parekh, and D. M. Tilbury, *Feedback Control of Computing Systems*. USA: Wiley & Sons, 2004.
- [11] F. S. Samani, K. Hammar, and R. Stadler, "Online policy adaptation for networked systems using rollout," in *NOMS 2024-2024 IEEE Network Operations and Management Symposium*, 2024, pp. 1–9.
- [12] T. A. Johansen and B. A. Foss, "Identification of non-linear system structure and parameters using regime decomposition," *Automatica*, vol. 31, no. 2, pp. 321–326, 1995.
- [13] C. E. Rasmussen and C. K. I. Williams, *Gaussian Processes for Machine Learning*. The MIT Press, 2006.
- [14] P. Koepernik and F. Pfaff, "Consistency of Gaussian process regression in metric spaces," *Journal of Machine Learning Research*, vol. 22, no. 244, pp. 1–27, 2021.
- [15] C. Oh, J. M. Tomczak, E. Gavves, and M. Welling, *Combinatorial Bayesian optimization using the graph cartesian product*. Red Hook, NY, USA: Curran Associates Inc., 2019.
- [16] D. Bertsekas, *Rollout, Policy Iteration, and Distributed Reinforcement Learning*, ser. Athena scientific optimization and computation series. Athena Scientific, 2021.
- [17] —, "Rollout algorithms and approximate dynamic programming for Bayesian optimization and sequential estimation," 2022, <https://arxiv.org/abs/2212.07998>.
- [18] K. Hammar, Y. Li, T. Alpcan, E. C. Lupu, and D. Bertsekas, "Adaptive network security policies via belief aggregation and rollout," 2025, <https://arxiv.org/abs/2507.15163>.
- [19] K. Hammar, T. Alpcan, and E. C. Lupu, "Incident response planning using a lightweight large language model with reduced hallucination," 2025, <https://arxiv.org/abs/2508.05188>.
- [20] K. Hammar and T. Li, "Online incident response planning under model misspecification through Bayesian learning and belief quantization," in *Proceedings of the 2025 Workshop on Artificial Intelligence and Security*, ser. AISC '25. New York, NY, USA: Association for Computing Machinery, 2025, preprint: <https://arxiv.org/abs/2508.14385>.
- [21] D. Bertsekas, *Reinforcement learning and optimal control*. Athena Scientific, 2019.
- [22] —, *Abstract Dynamic Programming*. Athena Scientific, 2018.
- [23] R. Storn and K. Price, "Differential evolution – a simple and efficient heuristic for global optimization over continuous spaces," *Journal of Global Optimization*, vol. 11, no. 4, pp. 341–359, Dec 1997.
- [24] Flask community, "Flask," [Online]. Available at: <https://flask.palletsprojects.com/en/2.1.x/>, Accessed on: June 7, 2022.
- [25] Kubernetes community, "Production-grade container orchestration," 2014. [Online]. Available at: <https://kubernetes.io/>, Accessed on: June 7, 2022.
- [26] Istio community, "Simplify observability, traffic management, security, and policy with the leading service mesh," 2017. [Online]. Available at: <https://istio.io/>, Accessed on: June 7, 2022.
- [27] MongoDB community, "Mongodb," 2009. [Online]. Available at: <https://www.mongodb.com/>, Accessed on: June 7, 2022.
- [28] D. Mills, "Internet time synchronization: the network time protocol," *IEEE Transactions on Communications*, vol. 39, no. 10, pp. 1482–1493, 1991.
- [29] K. Hammar and F. S. Samani, "Source code and traces for the paper "Online identification of IT systems through active causal learning"," 2025, <https://github.com/Limmen/csle> and https://github.com/foroughsh/online_policy_adaptation_using_rollout.
- [30] K. Hammar and R. Stadler, "Intrusion prevention through optimal stopping," *IEEE Transactions on Network and Service Management*, vol. 19, no. 3, pp. 2333–2348, 2022.
- [31] —, "Learning near-optimal intrusion responses against dynamic attackers," *IEEE Transactions on Network and Service Management*, vol. 21, no. 1, pp. 1158–1177, 2024.
- [32] —, "Digital twins for security automation," in *NOMS 2023-2023 IEEE/IFIP Network Operations and Management Symposium*, 2023, pp. 1–6.
- [33] K. Hammar, "Optimal security response to network intrusions in IT systems," Ph.D. dissertation, KTH Royal Institute of Technology, 2024.
- [34] F. S. Samani, R. Stadler, C. Flinta, and A. Johnsson, "Conditional density estimation of service metrics for networked services," *IEEE Transactions on Network and Service Management*, vol. 18, no. 2, pp. 2350–2364, 2021.
- [35] B. C. Tedeschi, G. Kwon, M. Nicoli, and M. Z. Win, "Real-time Bayesian neural networks for 6G cooperative positioning and tracking," *IEEE Journal on Selected Areas in Communications*, vol. 42, no. 9, pp. 2322–2338, 2024.

- [36] E. Snelson and Z. Ghahramani, "Local and global sparse Gaussian process approximations," in *Proceedings of the Eleventh International Conference on Artificial Intelligence and Statistics*, ser. Proceedings of Machine Learning Research, M. Meila and X. Shen, Eds., vol. 2. San Juan, Puerto Rico: PMLR, 21–24 Mar 2007, pp. 524–531.
- [37] A. Damianou and N. D. Lawrence, "Deep Gaussian processes," in *Proceedings of the Sixteenth International Conference on Artificial Intelligence and Statistics*, ser. Proceedings of Machine Learning Research, C. M. Carvalho and P. Ravikumar, Eds., vol. 31. Scottsdale, Arizona, USA: PMLR, 29 Apr–01 May 2013, pp. 207–215.
- [38] A. Gammernan and V. Vovk, "Hedging predictions in machine learning," *The Computer Journal*, vol. 50, no. 2, pp. 151–163, 2007.
- [39] V. Vovk, A. Gammernan, and G. Shafer, *Algorithmic Learning in a Random World*. Berlin, Heidelberg: Springer-Verlag, 2005.
- [40] R. Garnett, *Bayesian Optimization*. Cambridge University Press, 2023.
- [41] L. Ljung, *System identification (2nd ed.): theory for the user*. USA: Prentice Hall PTR, 1999.
- [42] K. J. Åström and P. Eykhoff, "System identification—a survey," *Automatica*, vol. 7, no. 2, pp. 123–162, 1971.
- [43] B. Wahlberg, "System identification using Kautz models," *IEEE Transactions on Automatic Control*, vol. 39, no. 6, pp. 1276–1282, 2002.
- [44] Y. Jedra and A. Proutiere, "Finite-time identification of linear systems: Fundamental limits and optimal algorithms," *IEEE Transactions on Automatic Control*, vol. 68, no. 5, pp. 2805–2820, 2023.
- [45] M. Araya-López, O. Buffet, V. Thomas, and F. Charpillet, "Active learning of MDP models," in *European Workshop on Reinforcement Learning*. Springer, 2011, pp. 42–53.
- [46] R. S. Sutton and A. G. Barto, *Introduction to Reinforcement Learning*, 1st ed. Cambridge, MA, USA: MIT Press, 1998.
- [47] R. S. Sutton, "Dyna, an integrated architecture for learning, planning, and reacting," *ACM Sigart Bulletin*, vol. 2, no. 4, pp. 160–163, 1991.
- [48] T. Alpcan and I. Shames, "An information-based learning approach to dual control," *IEEE Transactions on Neural Networks and Learning Systems*, vol. 26, no. 11, pp. 2736–2748, 2015.
- [49] P. Kumar, "Simultaneous identification and adaptive control of unknown systems over finite parameter sets," *IEEE Transactions on Automatic Control*, vol. 28, no. 1, pp. 68–76, 1983.
- [50] R. Sutton, A. Barto, and R. Williams, "Reinforcement learning is direct adaptive optimal control," *IEEE Control Systems Magazine*, vol. 12, no. 2, pp. 19–22, 1992.
- [51] K. J. Åström and B. Wittenmark, *Adaptive Control*, 2nd ed. USA: Addison-Wesley Longman Publishing Co., Inc., 1994.
- [52] D. Bertsekas and I. Rhodes, "Sufficiently informative functions and the minimax feedback control of uncertain dynamic systems," *IEEE Transactions on Automatic Control*, vol. 18, no. 2, pp. 117–124, 1973.
- [53] Z. Pan and T. Basar, "Adaptive controller design for tracking and disturbance attenuation in parametric strict-feedback nonlinear systems," *IEEE Transactions on Automatic Control*, vol. 43, no. 8, pp. 1066–1083, 1998.
- [54] I. Ziemann and H. Sandberg, "Regret lower bounds for unbiased adaptive control of linear quadratic regulators," *IEEE Control Systems Letters*, vol. 4, no. 3, pp. 785–790, 2020.
- [55] K. Åström and B. Wittenmark, "On self tuning regulators," *Automatica*, vol. 9, no. 2, pp. 185–199, 1973.
- [56] H. Mania, M. I. Jordan, and B. Recht, "Active learning for nonlinear system identification with guarantees," *J. Mach. Learn. Res.*, vol. 23, no. 1, Jan. 2022.
- [57] R. Bellman and R. Kalaba, "On adaptive control processes," *IRE Transactions on Automatic Control*, vol. 4, no. 2, pp. 1–9, 1959.
- [58] V. Aglietti, X. Lu, A. Paleyes, and J. González, "Causal Bayesian optimization," in *Proceedings of the Twenty Third International Conference on Artificial Intelligence and Statistics*, ser. Proceedings of Machine Learning Research, S. Chiappa and R. Calandra, Eds., vol. 108. PMLR, 26–28 Aug 2020, pp. 3155–3164.
- [59] V. Aglietti, N. Dhir, J. González, and T. Damoulas, "Dynamic causal Bayesian optimization," *Advances in Neural Information Processing Systems*, vol. 34, pp. 10 549–10 560, 2021.
- [60] S. Sussex, A. Makarova, and A. Krause, "Model-based causal Bayesian optimization," *arXiv preprint arXiv:2211.10257*, 2022.
- [61] J. Zhang, L. Cammarata, C. Squires, T. P. Sapsis, and C. Uhler, "Active learning for optimal intervention design in causal models," *Nature Machine Intelligence*, vol. 5, no. 10, pp. 1066–1075, Oct 2023.
- [62] L. Gultchin, V. Aglietti, A. Bellot, and S. Chiappa, "Functional causal Bayesian optimization," in *Proceedings of the Thirty-Ninth Conference on Uncertainty in Artificial Intelligence*, ser. Proceedings of Machine Learning Research, R. J. Evans and I. Shpitser, Eds., vol. 216. PMLR, 31 Jul–04 Aug 2023, pp. 756–765.
- [63] Y.-B. He and Z. Geng, "Active learning of causal networks with intervention experiments and optimal designs," *Journal of Machine Learning Research*, vol. 9, no. 84, pp. 2523–2547, 2008.
- [64] K. Greenewald, D. Katz, K. Shanmugam, S. Magliacane, M. Kocaoglu, E. Boix Adsera, and G. Bresler, "Sample efficient active learning of causal trees," in *Advances in Neural Information Processing Systems*, H. Wallach, H. Larochelle, A. Beygelzimer, F. d'Alché-Buc, E. Fox, and R. Garnett, Eds., vol. 32. Curran Associates, Inc., 2019.
- [65] P. K. Rubenstein, I. Tolstikhin, P. Hennig, and B. Schölkopf, "Probabilistic active learning of functions in structural causal models," 2017, <https://arxiv.org/abs/1706.10234>.
- [66] D. Linzner and H. Koepl, "Active learning of continuous-time Bayesian networks through interventions," in *Proceedings of the 38th International Conference on Machine Learning*, ser. Proceedings of Machine Learning Research, M. Meila and T. Zhang, Eds., vol. 139. PMLR, 18–24 Jul 2021, pp. 6692–6701.
- [67] V. Aglietti, T. Damoulas, M. Álvarez, and J. González, "Multi-task causal learning with Gaussian processes," in *Advances in Neural Information Processing Systems*, H. Larochelle, M. Ranzato, R. Hadsell, M. Balcan, and H. Lin, Eds., vol. 33. Curran Associates, Inc., 2020, pp. 6293–6304.
- [68] C. Toth, L. Lorch, C. Knoll, A. Krause, F. Pernkopf, R. Peharz, and J. von Kügelgen, "Active Bayesian causal inference," in *Advances in Neural Information Processing Systems*, S. Koyejo, S. Mohamed, A. Agarwal, D. Belgrave, K. Cho, and A. Oh, Eds., vol. 35. Curran Associates, Inc., 2022, pp. 16 261–16 275.
- [69] S. Tong and D. Koller, "Active learning for parameter estimation in Bayesian networks," in *Advances in Neural Information Processing Systems*, T. Leen, T. Dietterich, and V. Tresp, Eds., vol. 13. MIT Press, 2000.
- [70] K. Hammar, N. Dhir, and R. Stadler, "Optimal defender strategies for CAGE-2 using causal modeling and tree search," 2024, <https://arxiv.org/abs/2407.11070>.
- [71] A. Andrew, S. Spillard, J. Collyer, and N. Dhir, "Developing optimal causal cyber-defence agents via cyber security simulation," *arXiv preprint arXiv:2207.12355*, 2022.
- [72] C. Yagemann, M. Pruett, S. P. Chung, K. Bittick, B. Saltaformaggio, and W. Lee, "{ARCUS}: symbolic root cause analysis of exploits in production systems," in *30th USENIX Security Symposium (USENIX Security 21)*, 2021, pp. 1989–2006.
- [73] A. Ikram, S. Chakraborty, S. Mitra, S. Saini, S. Bagechi, and M. Kocaoglu, "Root cause analysis of failures in microservices through causal discovery," in *Advances in Neural Information Processing Systems*, S. Koyejo, S. Mohamed, A. Agarwal, D. Belgrave, K. Cho, and A. Oh, Eds., vol. 35. Curran Associates, Inc., 2022, pp. 31 158–31 170.
- [74] Y. Liu, M. Zhang, D. Li, K. Jee, Z. Li, Z. Wu, J. Rhee, and P. Mittal, "Towards a timely causality analysis for enterprise security," in *25th Annual Network and Distributed System Security Symposium, NDSS 2018, San Diego, California, USA, February 18-21, 2018*. The Internet Society, 2018.
- [75] H. Zhang, D. D. Yao, N. Ramakrishnan, and Z. Zhang, "Causality reasoning about network events for detecting stealthy malware activities," *computers & security*, vol. 58, pp. 180–198, 2016.